Multiscale modelling of nanostructures

2004 J. Phys.: Condens. Matter 16 R1537

(http://iopscience.iop.org/0953-8984/16/50/R01)

INSTITUTE OF PHYSICS PUBLISHING JOURNAL OF PHYSICS: CONDENSED MATTER

J. Phys.: Condens. Matter **16** (2004) R1537–R1576 PII: S0953-8984(04)55699-0

TOPICAL REVIEW

Multiscale modelling of nanostructures

Dimitri D Vvedensky

The Blackett Laboratory, Imperial College, London SW7 2BZ, UK

Received 31 August 2004
Published 3 December 2004
Online at stacks.iop.org/JPhysCM/16/R1537
doi:10.1088/0953-8984/16/50/R01

Abstract

Most materials phenomena are manifestations of processes that are operative over a vast range of length and time scales. A complete understanding of the behaviour of materials thereby requires theoretical and computational tools that span the atomic-scale detail of first-principles methods and the more coarse-grained description provided by continuum equations. Recent efforts have focused on combining traditional methodologies—density functional theory, molecular dynamics, Monte Carlo methods and continuum descriptions—within a unified multiscale framework. This review covers the techniques that have been developed to model various aspects of materials behaviour with the ultimate aim of systematically coupling the atomistic to the continuum descriptions. The approaches described typically have been motivated by particular applications but can often be applied in wider contexts. The self-assembly of quantum dot ensembles will be used as a case study for the issues that arise and the methods used for all nanostructures. Although quantum dots can be obtained with all the standard growth methods and for a variety of material systems, their appearance is a quite selective process, involving the competition between equilibrium and kinetic effects, and the interplay between atomistic and long-range interactions. Most theoretical models have addressed particular aspects of the ordering kinetics of quantum dot ensembles, with far fewer attempts at a comprehensive synthesis of this inherently multiscale phenomenon. We conclude with an assessment of the current status of multiscale modelling strategies and highlight the main outstanding issues.

Contents

1. Introduction 1538
2. Hierarchy of methods for materials modelling 1541
   2.1. First-principles methods 1543
   2.2. Molecular dynamics 1545
   2.3. Monte Carlo methods 1546
   2.4. Continuum equations 1548

3. Methods of multiscale modelling 1550
3.1. Sequential parametrization 1550
3.2. Interface propagation 1553
3.3. Hybrid methods 1556
3.4. Coarse graining of atomistic degrees of freedom 1558
4. A case study: self-organized quantum dots 1563
4.1. First-principles studies of InAs/GaAs(001) heteroepitaxy 1564
4.2. Hybrid molecular dynamics–finite element calculation of strain in nanopixels 1565
4.3. Off-lattice kinetic Monte Carlo simulations of Stranski–Krastanov growth 1565
4.4. Nonlinear evolution equation for self-organization 1567
5. Summary and outlook 1568
Acknowledgments 1569
References 1569

1. Introduction

The technological hallmark of all civilizations is borne by the available raw materials that can be harnessed for practical uses. The Stone Age, Bronze Age and Iron Age all attest to the overriding importance of particular materials that artisans formed into weapons, tools and utensils, and artists crafted into signatures and snapshots of their culture. The second half of the 20th century will undoubtedly come to be known as the 'silicon age', as a testament to the pivotal role of this material in the information revolution. The relentless advance of materials technology continues unabated, driven by the expanding horizon of our demands and fuelled by aspirations of atom-by-atom assembly from the palette of the periodic table [1–3]. Smaller, faster computers, mobile telecommunications, terahertz materials, stronger, lighter structural materials, biocompatibility, tissue engineering . . .; the list goes on and on.

At the heart of materials development are the processing and characterization methodologies for the control of structure, functionality and properties. The sophistication of modern technology has reached the point where, in many cases, the operational consequences of atomic-scale phenomena have a direct impact on the design process. We consider a traditional example, the deformation behaviour of materials. Dislocations, which appear as extra or displaced planes of atoms inserted into a regular lattice, allow materials to deform without brittle fracture. An important property of dislocations is their ability to move through the lattice in response to an applied external stress, thereby allowing slip to propagate. Dislocations and other defects in crystals correspond to specific atomic configurations whose energies can be calculated from quantum mechanical principles, and there has been considerable progress in this direction [4–6].

In a more coarse-grained view of deformation, the interactions between dislocations and their movement within and across grains are mediated by long-range elastic fields that do not require full atomic resolution. The dislocations can be considered as the basic elements of a grain-size model in which their interactions are determined by a combination of linear elasticity and atomistic simulations. Such simulations describe the collective behaviour of a large number of dislocations and provide direct real-space information about their microstructure as a function of applied stress [7, 8]. At the macroscopic scale, the deformation of the material is calculated from the interactions between grains. Indeed, polycrystalline grains may themselves be considered as the basic interacting elements in a simulation of deformation [9].

The foregoing 'bottom-up' example contrasts with the following 'top-down' scenario. The dawn of the electronics age was heralded by the invention of the transistor in the late

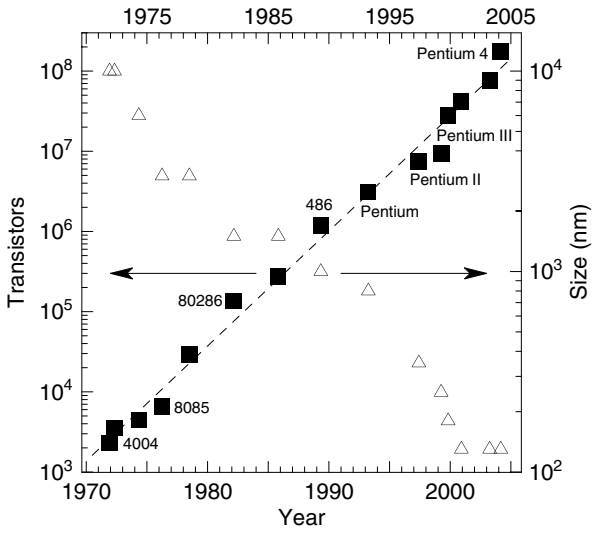

Figure 1. A semi-log plot of the number of transistors on a silicon chip (filled squares, left scale) and their minimum feature size (open triangles, right scale) as a function of their announcement dates by Intel since 1971 [13]. The names of several processors are indicated. The broken line is a least squares fit and corresponds to Moore's law with a doubling time of two years. The Semiconductor Industry Association Roadmap [14] predicts that feature sizes of 70 nm will be achieved by 2008.

1940s. Much smaller than vacuum tubes, transistors also had much shorter switching times and consumed much less power. Accordingly, electronic circuits that used transistors could be made faster and more complex than those based on vacuum tubes. Further improvements necessitated making the transistors smaller and placing them closer together. The key for miniaturization was the development of the integrated circuit in the late 1950s. The idea was to fabricate patterned layers of materials with different electrical properties on top of one another on a 'chip' of silicon to form the various circuit elements, such as transistors and capacitors, together with their electrical connections. The patterning of the layers is carried out by the selective removal of material using lithography, for example, with light that has been focused with a lens.

Since the early 1970s the number of transistors that semiconductor manufacturers can put on a chip has on average doubled every two years (figure 1). This is known as Moore's law, named after Gordon Moore (one of the co-founders of Intel), who made this observation in 1965 [10]. This exponential increase in transistor densities has been sustained largely on the back of improvements in lithographic technology, which has seen dramatic reductions in the feature size, from several microns to a few tenths of a micron, as shown in figure 1. This increase has been accomplished without corresponding increases in production costs [11]. The result is processors with larger memories and faster operating speeds which, for the consumer, translates into more powerful, but less expensive, computers.

But the physical principles underlying chip production suggest that there are obstacles to the unabated progression of Moore's law [12]. As the thickness of the conventional SiO_2 insulator continues to be reduced, electrons will eventually be able to tunnel directly through the thin film, at which point the consequent increases in power consumption and heat production become critical issues. Current estimates are for minimum feature sizes of

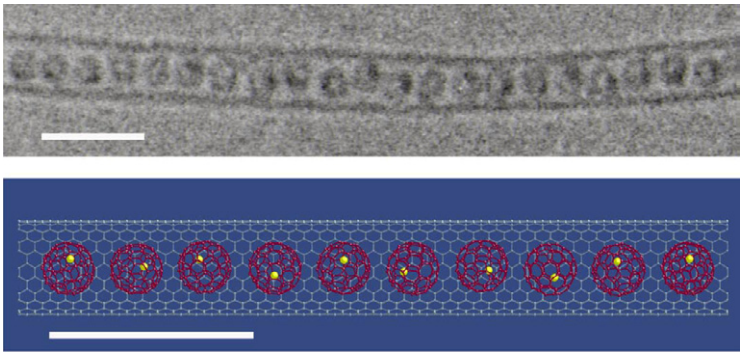

Figure 2. An electron micrograph [19] of an isolated nanotube into which a chain of Gd metallofullerenes has been inserted (top) and a schematic representation of the structure (bottom). The horizontal bars represent a length of 3 nm. Reprinted with permission from K Suenaga, M Tencé, C Mory, C Colliex, H Kato, T Okazaki, H Shinohara, K Hirahara, S Bandow and S Iijima 2000 *Science* **290** 2280. Copyright 2000 AAAS.

20–30 nm being achieved around 2018. However, new materials, new architectures and new computing paradigms could extend the life of Moore's law [11].

The drive toward miniaturization is not likely to cease until the materials and components that will replace the metal–oxide–semiconductor-based technology are assembled at the atomic scale. An important step toward this goal was the discovery [15] of carbon nanotubes (figure 2), which consist of graphitic layers seamlessly wrapped into cylinders only a few nanometres in diameter, but extending up to millimetres in length. These systems are endowed with extraordinary structural, mechanical and electrical properties that are derived from the nature of the carbon bond, their cylindrical symmetry and their quasi-one-dimensionality. For example, nanotubes can sustain quite large deformations reversibly, and multiwalled nanotubes have been reported to have a Young's modulus more than an order of magnitude greater than that of steel [16, 17]. Such remarkable properties have led to research into the functionalization of nanotubes by particles inserted into their hollow interior, including biological molecules, thus creating the potential for a broad range of electronic, optical and biotechnological applications [18].

An altogether different avenue for modern materials science and technology is found in biological applications. For example, the sequence of events following a medical implant [20] is initiated by the interactions between individual water molecules and the surface of the implant, which occurs on a timescale of nanoseconds. The resulting water 'shell' is an important factor for influencing proteins and other molecules that arrive later, on a timescale of microseconds to milliseconds. Eventually, the cells reaching the surface interact through the protein coating whose properties are determined by the initial surface and the water adlayer.

These examples provide somewhat opposing views about the multiscale nature of materials behaviour. At the root of the 'bottom-up' approach is quantum mechanics. All other methods at more coarse-grained length and time scales are approximations to the quantum mechanical description of materials. The goal is to predict macroscopic behaviour directly from quantum mechanical principles, if the calculation can be carried out, or indirectly, when used in conjunction with other methods, which is the typical case. In the 'top-down' scheme, smaller structures mean that surfaces and interfaces gain importance in determining the properties of these structures because of the increasing surface-to-volume ratio. A greater understanding is therefore required of the relationships between structure, thermodynamics and properties

of surfaces and interfaces, especially for the chemical, structural, mechanical and thermal stability of small structures. For individual structures, a full quantum mechanical calculation may be feasible, but a multiscale approach is required for modelling an ensemble of structures and the interactions of these structures with their environment.

There are several reasons for the emergence of multiscale modelling as a theme for modern computational materials science. The first is the existence of fundamentally multiscale materials phenomena, such as crack initiation and propagation, which are characterized by a continuous feedback between atomic-scale and coarse-grained degrees of freedom, similar to that found in turbulence and critical phenomena. The second is the characterization of phenomena that have a firm conceptual basis at the macroscopic level, but have quite different manifestations at the atomic level, which significantly affects the properties of nanostructures. Examples include the competition between interfacial energy and 'bulk' morphological stability, stress and strain inhomogeneities that affect dopant distributions in semiconductor nanostructures, including the electrical characteristics of resonant tunnelling diodes, and dislocation dynamics and deformation processes. Another reason is that, with improvements in computer hardware and software, such calculations have become feasible and are now capable of addressing many issues uncovered by experiments with successively finer resolutions.

Multiscale modelling also has much to offer the practical development and optimization of materials. Experimental methods of materials design and synthesis are costly and time-consuming, leading to long development times. Modelling and simulation can be used to optimize processing parameters and to interpret experiments at the atomic scale. This is especially important for situations where phenomena are too fast or too complex to image directly. On the other hand, simulations based on large-scale quantum mechanical calculations and molecular dynamics can be stopped at any time, examined to whatever level of detail is required (which may involve advanced data management and visualization techniques [21]) and used to suggest modifications based on fundamental principles.

The organization of this review is as follows. In section 2 we summarize the main traditional methods for modelling materials. Each method has been developed and optimized for space and time scales appropriate to particular degrees of freedom, from electrons and nuclei to coarse-grained fields. With this background, we discuss several strategies for the multiscale modelling of materials in section 3. All of these rely on the methods in section 2, but differ in the way that information from each length scale is incorporated. Many aspects of nanostructures provide fertile ground for multiscale methodologies, and in section 4 we discuss applications to quantum dots. The interplay between the formation kinetics of individual quantum dots and the properties of quantum dot ensembles provides a paradigm for all nanostructures. We conclude with a discussion of the outstanding issues in section 5. Multiscale modelling is an expanding effort that now finds application in a number of disciplines. There have been several recent conference proceedings [22–24], review articles [25–29], and special issues [30] that are devoted to particular aspects of this effort. In addition to nanostructured materials, multiscale methods have also been developed for fluid flow through porous media [31, 32], and abstract interacting particle systems [33–35].

2. Hierarchy of methods for materials modelling

The most common approach to materials modelling is based on the 'divide and conquer' strategy, wherein methods appropriate to particular length and time scales are used to address aspects of materials phenomena that operate only over those scales. This has led to several independent methodological streams, which can be broadly categorized as *ab initio* density

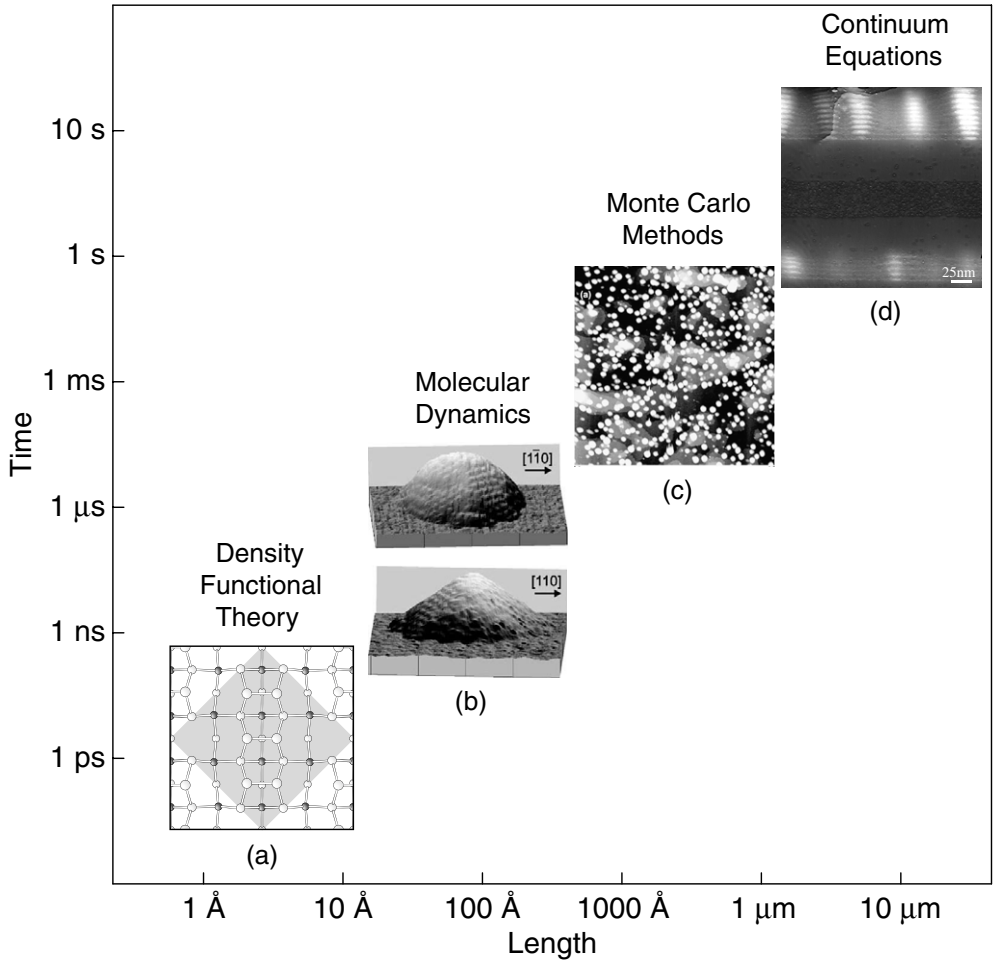

Figure 3. The hierarchy of modelling methods that are discussed in section 2 for the range of length and time scales over which they typically used, illustrated with the multiscale phenomenology of quantum dots obtained from the heteroepitaxial growth of InAs on GaAs(001). (a) The c(4 × 4) phase (reconstruction) of the GaAs(001) surface that is the most common substrate for the growth of quantum dots in this system [36, 37]. The unit cell is indicated by the shaded region. (b) Atomically resolved scanning tunnelling microscopy (STM) images (200 Å × 200 Å) of a single three-dimensional island along [1$\bar{1}$0] and [110], showing a lens shape in the top panel, but bounding (137) facets in the bottom panel [38]. Reprinted from K Jacobi 2003 Atomic structure of InAs quantum dots on GaAs *Prog. Surf. Sci.* **71** 185–215. Copyright 2003, with permission from Elsevier. (c) An STM image (500 nm × 500 nm) of an ensemble of three-dimensional islands on GaAs(001) grown with a substrate temperature of 450 °C and a growth rate of 0.05 Å s^{-1} [38]. The number density of the dots is 1.9×10^{11} cm^{-1}. Reprinted from K Jacobi 2003 Atomic structure of InAs quantum dots on GaAs *Prog. Surf. Sci.* **71** 185–215. Copyright 2003, with permission from Elsevier. (d) A (200 nm × 200 nm) section of a large-scale cross-sectional image showing five- and ten-period superlattices of InAs/GaAs quantum dots (bright regions) [39]. The lower boundaries of each image define the basic spatial and temporal resolutions of the corresponding computational method. The upper boundaries are determined by computational and algorithmic limits; continuum equations extend beyond the limits shown into the macroscopic domain.

functional theory, molecular dynamics, statistical methods based on Monte Carlo algorithms and continuum mechanics (figure 3). Each of these is computationally intensive in its own right,

so most of the initial effort was directed to optimizing algorithms, potentials and parameters for each method individually, rather than generating information for input into other methods. However, the expanding capabilities of computational methods due to the increasing power of computers and continuing development of efficient algorithms, together with advances in the synthesis, analysis and visualization of materials at increasingly finer spatial and temporal resolutions, has spawned a huge effort in the multiscale descriptions of materials phenomena. In this section, we describe the building blocks of these methods. The following section will describe how these are combined within multiscale modelling strategies.

2.1. First-principles methods

The observable properties of solids are governed by quantum mechanics, as expressed by solutions of a Schrödinger equation for the motion of the electrons and the nuclei. However, because of the inherent difficulty of obtaining even grossly approximate solutions of the full many-body Schrödinger equation, one typically focuses on reduced descriptions that are believed to capture the essential energetics of the problem of interest.

Hohenberg, Kohn and Sham [40–42] formulated a theory based on the electron density, in terms of which the solution of the Schrödinger equation could be given a sound mathematical basis. This method is based on two theorems:

(i) the total energy of an electron system in an external potential is a unique functional of the total electron density; and
(ii) the density that minimizes the energy is the ground-state density, and this minimum energy is the ground-state energy of the system.

The basic idea of the Kohn–Sham–Hohenberg theorems is that the 'real' electrons are replaced by 'effective' electrons with the same total density that move as *independent* particles in the potential generated by the other electrons and ion cores. For a system of N electrons, the total density ϱ is expressed as a sum of the orbitals ψ_i as

$$\varrho(\mathbf{r}) = \sum_{i=1}^{N} |\psi_i(\mathbf{r})|^2, \tag{1}$$

where the ψ_i are solutions of the Kohn–Sham equations,

$$\left[-\frac{\hbar^2}{2m}\nabla^2 + V_{\text{eff}}\right]\psi_i(\mathbf{r}) = \varepsilon_i\psi_i(\mathbf{r}), \tag{2}$$

in which the effective potential V_{eff} is the sum of Coulomb and exchange–correlation contributions. The Coulomb potential V_{C} is

$$V_{\text{C}}(\mathbf{r}) = -e^2\int \frac{\varrho(\mathbf{r}')}{|\mathbf{r}-\mathbf{r}'|}\,\mathrm{d}\mathbf{r} + e^2\sum_{\alpha}\frac{Z_\alpha}{|\mathbf{R}_\alpha - \mathbf{r}|}, \tag{3}$$

in which $\mathbf{R}_\alpha$ denotes atomic positions. This potential is a solution of Poisson's equation and thus has a purely classical origin. The exchange–correlation potential V_{xc} is obtained from the exchange–correlation energy E_{xc} via

$$V_{\text{xc}} = \frac{\delta E_{\text{xc}}[\varrho(\mathbf{r})]}{\delta\varrho}. \tag{4}$$

The solution of these equations for the individual electrons must be obtained self-consistently because the wavefunction for each electron is included in the effective potential of all other electrons.

The Kohn–Sham–Hohenberg theory, now called density functional theory (DFT), provides an enormous conceptual and computational simplification of the many-electron problem. The complex interactions between the electrons of the original system are subsumed into a universal energy functional. But the Hohenberg–Kohn–Sham theorems are only statements about *existence* and *uniqueness*: they do not provide a prescription for determining this functional which, because of the exchange–correlation energy, is not generally known. The widely adopted local density approximation (LDA) presumes that this functional depends only on the *local* value of electron density [41], i.e. that inhomogeneous electron systems can be viewed as locally homogeneous. The local density functional has been studied in a system of interacting electrons with a constant density (because of the homogeneous background of positive charge rendering the system electrically neutral), called the *homogeneous electron gas*, with several approaches, including quantum Monte Carlo methods [43], which produces results that are essentially exact.

The success of the LDA has far exceeded initial expectations [41]. For systems with slowly varying charge densities, as in many metals, the LDA has proven to be an accurate approximation, with bond lengths and angles calculated to within a few per cent of their experimentally measured values. There are several reasons for this success, including the fact that, although the shape of the exchange–correlation hole—the region surrounding each electron that repels the other electrons—is not well represented, the overall effective charge is described exactly [44, 45], and the errors made by the LDA for exchange and correlation separately tend to cancel [46, 47]. But there are also known limitations of the LDA. Errors are incurred when treating systems away from equilibrium configurations, as in the calculation of transitions rates. For nonuniform charge densities the exchange–correlation energy can deviate significantly from the uniform limit. The generalized gradient approximation (GGA) [48–51] employs the gradient of the charge density to account for local variations in the electron density. For systems where the charge density is sufficiently slowly varying, the GGA provides an improvement over the LDA.

Density functional theory is suitable for calculating the charge density and energy for a fixed structure of atoms but is inefficient if the atoms are allowed to move as, for example, during the geometrical optimization of a molecule or solid. Car and Parrinello [52] proposed a method based on the DFT framework to overcome this limitation. The energy minimization is carried out by constructing equations of motion for all of the parameters involved in the variation, including the nuclear coordinates for geometrical optimization, and the electronic wavefunctions are updated simultaneously with the position changes of the atomic nuclei. The efficiency of this scheme [53] has considerably expanded the system sizes accessible to static calculations and has opened up the possibility of *ab initio* 'quantum' molecular dynamics simulations. When the electronic wavefunctions are reliably known, the forces on the atomic nuclei can be obtained from the Hellmann–Feynman theorem and then used to move the atoms as in standard molecular dynamics (section 2.2).

The development of efficient algorithms and a better understanding of density functionals [54] have made DFT the primary method for calculating the properties of materials [55], including band structures, band gaps, cohesive energies, chemisorption energies, catalytic properties and activation barriers for various kinetic processes. System sizes of several hundred atoms are well within the scope of modern methods, but the scaling of the required computer time as the square of the number of atoms in the calculation has prevented more rapid progress. This has stimulated the search for 'order-N' methods, where the computer time scales approximately *linearly* with N, by exploiting the inherent locality of quantum mechanics [56–58]. The implementation of this strategy will place many important systems in nanotechnology within the capabilities of DFT.

2.2. Molecular dynamics

Quantum molecular dynamics simulations are limited to system sizes of a few hundred atoms and to elapsed real times of a few picoseconds. Accordingly, the first step in the coarse graining of the full quantum mechanical description of a dynamical process is to remove the electronic degrees of freedom from the problem. This is accomplished by first using the Born–Oppenheimer approximation to separate the electronic and nuclear coordinates. The total energy is then calculated for each set of N nuclear positions $\mathbf{R}_\alpha$, for $\alpha = 1, 2, \ldots, N$; from this the forces exerted on each atom by all other atoms can be determined. Interpolation between these points yields a potential energy surface $U(\{\mathbf{R}_\alpha\})$. Regarding the atoms as classical particles moving on this surface, the *quantum mechanical* motion governed by the Schrödinger equation is replaced by Newton's equation of *classical* mechanics:

$$\mathbf{F}_\alpha = m_\alpha \frac{\mathrm{d}^2\mathbf{R}_\alpha}{\mathrm{d}t^2}, \tag{5}$$

where m_α is the mass of the αth atom and the force $\mathbf{F}_\alpha$ acting on this atom is calculated from the interatomic potential energy according to

$$\mathbf{F}_\alpha = -\nabla_\alpha U. \tag{6}$$

Thus, the classical Hamiltonian $\mathcal{H}$ of the system is

$$\mathcal{H}_{\mathrm{MD}} = \tfrac{1}{2}\sum_\alpha m_\alpha \mathbf{V}_\alpha^2 + U, \tag{7}$$

where $\mathbf{V}_\alpha$ is the velocity of the αth atom. These are the equations of the molecular dynamics method [59–61].

There are two primary aspects to the practical implementation of molecular dynamics: (i) the numerical integration of the equations of motion together with the boundary conditions and any constraints on the system; and (ii) the choice of the potential. For a system of N particles, equation (5) represents a system of $3N$ second-order differential equations. This system can be expressed as $6N$ first-order differential equations by introducing the velocity as a separate variable:

$$\frac{\mathrm{d}\mathbf{R}_\alpha}{\mathrm{d}t} = \mathbf{V}_\alpha, \qquad \frac{\mathrm{d}\mathbf{V}_\alpha}{\mathrm{d}t} = \frac{\mathbf{F}_\alpha}{m_\alpha}. \tag{8}$$

The systems of equations (5) or (8) are solved numerically with finite difference methods to obtain the trajectories of the atoms on the potential energy surface. The most common integrators are based on the Verlet algorithm [62, 63] and its descendents, and predictor–corrector methods [64]. When applied to the system in equation (8), these algorithms are used to iteratively update the forces, the velocities and the positions over the timescale of the simulation. Parallel computing with spatial decomposition [61, 65] has extended the system sizes that can be studied with molecular dynamics to $N \sim 10^6$–10^9 [66, 67].

All of the physics in the molecular dynamics method is contained in the forces acting on each particle in the system, which are determined by the interatomic potentials in equation (6). For a single-component system, the potential energy U is first written as an expansion in terms of n-body potentials:

$$U(\{\mathbf{R}_\alpha\}) = \frac{1}{2!}\sum_{\alpha\neq\beta} U_2(\mathbf{R}_{\alpha\beta}) + \frac{1}{3!}\sum_{\alpha\neq\beta\neq\gamma} U_3(\mathbf{R}_{\alpha\beta}, \mathbf{R}_{\alpha\gamma}, \mathbf{R}_{\beta\gamma}) + \cdots. \tag{9}$$

Here, $\mathbf{R}_{\alpha\beta} = \mathbf{R}_\alpha - \mathbf{R}_\beta$ are interatomic separations and U_2 represents an n-body interaction energy. The two-body term U_2 represents the interaction between atomic pairs and depends only on their separation $\mathbf{R}_{\alpha\beta}$. This term describes the energetic cost of bond stretching. The

three-body term U_3 depends on the relative orientations of triplets of atoms, i.e. not simply upon interatomic *distances*, but on bond *angles* as well, and thereby accounts for the energetics of bond stretching *and* bond bending. For the expansion in equation (9) to be meaningful, convergence must be rapid in n, although most molecular dynamics studies truncate this expansion at either the second or the third order. Once the interaction potential has been specified, the time development of the system is calculated from the equations of motion (5) or (8).

The choice of potential for a molecular dynamics simulation is determined by factors such as the bond type, the desired accuracy, transferability and the available computational resources. Potentials can be categorized broadly as (i) pair potentials, (ii) empirical many-body potentials and (iii) quantum mechanical potentials. Two-body, or pair, potentials, such as the Lennard-Jones [68] and Morse [69] potentials, are used for large-scale simulations where computational efficiency is paramount, but where a generic description is sufficient, rather than detailed comparisons with a particular materials system. For systems where multibody interactions are important [70], the Stillinger–Weber [71], Tersoff [72, 73] and Brenner [74] potentials are often used for covalent materials, and embedded-atom [75, 76], effective medium [77] and Finnis–Sinclair potentials [78] are common choices for metals. Such potentials are empirical in that they are parametrized by fitting either to a set of experimental measurements or to quantum mechanical calculations of representative atomic configurations. Typical properties used for such parametrizations are the lattice constant, binding energy, elastic constants and vacancy formation energies. The basic assumption of this approach is that the fitting captures the essential features of the interatomic potential for the phenomenon of interest. However, large local departures from the coordination or bonding used for the parametrization can take such potentials outside their domain of validity and lead to unreliable results. This has fostered efforts at deriving interatomic potentials directly from quantum mechanical principles. Foremost among these are potentials based on [79, 80] and derived from [81, 82] tight-binding theory and those based on the Kohn–Sham equations using generalized pseudopotential theory [4, 83].

The basic limitation of the molecular dynamics method that has prevented long simulation times is that processes such as atomic diffusion are inherently multiscale phenomena. The integration time step must be small enough to capture the dynamics of the vibration modes of the system, with frequencies of the order of 10^{13} s^{-1}. This requires time steps in the *femtosecond* range. But the residence time of an adatom between hops is of the order of *microseconds*, and the interactions responsible for aggregation phenomena occur over a timescale of *milliseconds* to *minutes*. This 'time gap' is evident from the trajectories of atoms, which are complex orbitals localized around their initial sites with only rare excursions to neighbouring sites [84, 85]. Several methods have been developed for accelerating molecular dynamics with such rare events based on stimulating the transitions to occur faster than in an ordinary simulation [86]. In favourable circumstances, molecular dynamics simulations can be extended to microseconds.

2.3. Monte Carlo methods

The next step for coarse graining is to address the 'time gap' problem of molecular dynamics. The basis of Monte Carlo methods [87] is that the *deterministic* equations (5) of the molecular dynamics method are replaced by *stochastic* transitions for the slow processes in the system. The name 'Monte Carlo' was coined by John von Neumann [88] and refers to the random sampling of numbers, in analogy to gambling in Monte Carlo, Monaco, a city renowned for its casinos. In their most general form, Monte Carlo methods are stochastic algorithms

for exploring phase space, but their implementation for equilibrium and nonequilibrium calculations is somewhat different. We first review the Metropolis algorithm, which is the basis of applications to *equilibrium* systems.

2.3.1. The Metropolis algorithm. Consider the thermodynamic average $\langle y \rangle$ of a variable with values y_i in state i that has energy E_i,

$$\langle y \rangle = \frac{\sum_i y_i p_i}{\sum_i p_i}, \tag{10}$$

in which the probabilities $p_i = \mathrm{e}^{-E_i/k_\mathrm{B}T}$, where k_B is Boltzmann's constant and T is the absolute temperature. If the system is initially in a state i, detailed balance requires that the rate of transitions T_{ij} from state i to state j satisfies

$$p_i T_{ij} = p_j T_{ji}, \tag{11}$$

or

$$\frac{T_{ij}}{T_{ji}} = \frac{p_j}{p_i} = \mathrm{e}^{-(E_j - E_i)/k_\mathrm{B}T}. \tag{12}$$

The right-hand side of this equation is known, so to generate a set of states with the distribution p_i, the T_{ij} are chosen as

$$T_{ij} = \begin{cases} 1, & \text{if } p_j > p_i \quad (E_j < E_i); \\ \mathrm{e}^{-(E_j - E_i)/k_\mathrm{B}T}, & \text{if } p_j \leqslant p_i \quad (E_j \geqslant E_i). \end{cases} \tag{13}$$

A random number $r \in (0, 1)$ is then selected and the system is moved to state j only if $r < \mathrm{e}^{-(E_j - E_i)/k_\mathrm{B}T}$. This is the Metropolis algorithm [89, 90]. The 'dynamics' so produced does *not* represent the actual evolution of the system [91, 92].

2.3.2. Kinetic Monte Carlo simulations. Suppose that the probability of finding a system in state σ at time t is $P(\sigma, t)$ and that the rate of transitions per unit time from σ to σ' is $W(\sigma, \sigma')$. The equation of motion for P is the master equation [93]:

$$\frac{\partial P}{\partial t} = \sum_{\sigma'} P(\sigma', t) W(\sigma', \sigma) - \sum_{\sigma'} P(\sigma, t) W(\sigma, \sigma'). \tag{14}$$

Kinetic Monte Carlo (KMC) methods are algorithms that solve the master equation by accepting and rejecting transitions with probabilities that yield the correct evolution of a nonequilibrium system.

The KMC method represents an additional level of abstraction beyond the molecular dynamics method. The effect of fast dynamical events is taken into account by using stochastic transition rates for slower events. These transition rates are often represented as the product of an attempt rate and the probability of success per attempt, which is taken as an exponential involving the energy barrier to the process. Every event i is assigned a rate r_i:

$$r_i = \nu_i \exp(-E_i/k_\mathrm{B}T), \tag{15}$$

where ν_i is a frequency prefactor, typically of the order of a vibrational frequency (10^{13} s^{-1}) for surface processes [94, 95], E_i is the free energy barrier for the process and T is the absolute temperature. Although the details of the underlying mechanism for kinetic processes are lost, the explicit calculation of atomic trajectories is avoided, so KMC simulations can be performed over real times, running into seconds, hours or days, as required. In essence, the factor ν_i in equation (15) represents the timescale of the fastest process, which is computed explicitly in the molecular dynamics method, but the exponential factor increases this timescale in the

KMC method to that of the actual transitions. The KMC method thereby offers considerable advantages over the molecular dynamics method, both in terms of the real time over which the simulation evolves, and the number of atoms included in the simulation, because much of the computational overhead in molecular dynamics is used to evolve the system between rare events.

The construction of a model for a KMC simulation can often benefit from a related classical or quantum molecular dynamics simulation to identify the important physical process and estimate the prefactors and kinetic barriers. The transition rates are particular to the processes of interest and must be determined either by direct calculation, from a first-principles calculation or a molecular dynamics simulation, or inferred from experiment. The feasibility of performing detailed simulations over experimental timescales allows various parametrizations to be tested and models of kinetic phenomena to be validated. Such simulations play a key role in several multiscale modelling strategies.

A KMC simulation proceeds by tabulating all of the rates r_i and then advancing the system by a single configuration change chosen from all possible events. In the 'n-fold way' algorithm [96], this is achieved by first computing the total rate $R = \sum_i r_i$. A number $\xi_1 \in (0, 1)$ is then selected randomly, the integer n is identified such that

$$\sum_{i=1}^{n-1} \frac{r_i}{R} < \xi_1 \leqslant \sum_{i=1}^{n} \frac{r_i}{R} \tag{16}$$

and the system is updated by the execution of event n. The system clock is then advanced by choosing a second random number $\xi_2 \in (0, 1)$, whereupon the time of the simulation is advanced from t to $t + \Delta t$, where

$$\Delta t = -\frac{\ln \xi_2}{R}. \tag{17}$$

Recent advances [97, 98] using K-level searches and alternative data structures have led to significant improvements in the efficiency of Monte Carlo algorithms. Parallel algorithms [99, 100] have further extended the capabilities of the KMC method.

2.4. Continuum equations

Continuum equations, typically in the form of deterministic or stochastic partial differential equations, are at the pinnacle of the coarse-graining hierarchy. The underlying atomic structure of matter is neglected altogether and is replaced with a continuous and differentiable mass density. Analogous replacements are made for other physical quantities such as energy and momentum. Differential equations are then formulated either from basic physical principles, such as the conservation of energy or momentum, or by invoking approximations within a particular regime. For example, the standard equations of fluid mechanics are derived from conservation laws, but are asymptotically valid only in the limit where the timescales of molecular motion are much shorter than those of the fluid flow [101]. This can be justified for simple fluids, but not for fluids composed of complex molecules such as polymers. The rheology of complex fluids is modelled with constitutive relations that account for the deformation history of the fluid and acknowledge the molecular origins of deformation and flow.

There are many benefits of a continuum representation of materials phenomena. Foremost among these is the ability to examine macroscopic regions in space over extended periods of time. This is facilitated by extensive libraries of numerical methods for integrating deterministic and stochastic differential equations. The best known of these is the finite element method [102, 103]. This is a general method for solving differential equations whereby the

region of interest is tessellated with a uniform or nonuniform mesh determined by contiguous components called 'elements'. The solution of the differential equation is discretized on the mesh points, called nodes, and interpolated within the elements. A partial (respectively, ordinary) differential equation is thereby replaced by a set of coupled ordinary (respectively, algebraic) equations and solved numerically for the values of the solution at the nodal points. The main advantage of the finite element method is flexibility in geometric complexity, material inhomogeneities and anisotropies, all within a computationally efficient framework.

Consider the deformation of a material from a reference state $\mathbf{r}_0$ to a deformed state $\mathbf{r}$, which may vary with time. The displacement vector field $\mathbf{u}(\mathbf{r}, t)$ is defined in terms of these states as

$$\mathbf{u}(\mathbf{r}, t) = \mathbf{r}(t) - \mathbf{r}_0. \tag{18}$$

Within the framework of linear elasticity, the components ε_{ij} of the strain tensor are given in terms of the components (u_1, u_2, u_3) of $\mathbf{u}$ by

$$\varepsilon_{ij} = \tfrac{1}{2}\left(\partial_j u_i + \partial_i u_j\right), \tag{19}$$

where

$$\partial_k = \frac{\partial}{\partial r_k}, \tag{20}$$

and (r_1, r_2, r_3) are the components of $\mathbf{r}$. The Hamiltonian $\mathcal{H}$ is expressed as the sum of kinetic and potential energy contributions as

$$\mathcal{H} = \tfrac{1}{2}\int \varrho \dot{\mathbf{u}}^2 \,\mathrm{d}\mathbf{r} + \tfrac{1}{2}\int \varepsilon_{ij} C_{ijkl} \varepsilon_{kl} \,\mathrm{d}\mathbf{r}, \tag{21}$$

where ϱ is the mass density of the material, C_{ijkl} are the components of the elasticity tensor and summation is implied over repeated indices.

The finite element representation of the displacement field is defined at the nodes of the elements, and shape functions (sometimes called interpolation functions or basis functions) are used to extend this field throughout each element. Denoting by $\varphi_i(\mathbf{r})$ the shape function for the ith node, the displacement field is

$$\mathbf{u}(\mathbf{r}, t) = \sum_{i=1}^{N_\mathrm{n}} \varphi_i(\mathbf{r}) \mathbf{u}_i(t), \tag{22}$$

in which N_n is the number of nodes and $\mathbf{u}_i(t)$ is the displacement at the ith node. This relation implies two important properties of shape functions [102]: (i) a shape function takes the value 0 or 1 at a nodal point $\mathbf{r}_j$: $\varphi_i(\mathbf{r}_j) = \delta_{ij}$, where δ_{ij} is the Kronecker delta; and (ii) the sum of all shape functions at any point $\mathbf{r}$ is unity: $\sum_i \varphi_i(\mathbf{r}) = 1$. A common choice for the shape function is linear interpolation, whereby the basis function has the value unity at a given node and decreases to zero linearly at the nearest neighbour nodes, and is zero elsewhere. This is also a convenient choice for coupling to methods with atomic resolution because it permits a one-to-one correspondence between nodes and atoms. Upon substitution of equation (22) into (21), we obtain the finite element approximation to the elastic Hamiltonian:

$$\mathcal{H}_\mathrm{FE} = \tfrac{1}{2}\sum_{i,j=1}^{N_\mathrm{n}} \sum_{\ell=1}^{N_\mathrm{e}} \left(\dot{\mathbf{u}}_i^\ell M_{ij}^\ell \dot{\mathbf{u}}_j^\ell + \mathbf{u}_i^\ell K_{ij}^\ell \mathbf{u}_j^\ell\right), \tag{23}$$

where N_e is the number of elements and M and K are the finite element mass and stiffness matrices, respectively. For atomic-size elements, the mass can be collapsed onto the nodes rather than being uniformly distributed, in which case the mass matrix becomes diagonal: $M_{ij} = m_i \delta_{ij}$. Equations of motion for the displacement at the nodes, in the form of

a set of coupled ordinary differential equations, can now be obtained from the finite element Hamiltonian in terms of the forces from the surrounding nodes.

Complementing the numerical solution of partial differential equations is the vast analytic methodology for identifying asymptotic scaling regimes and performing stability analyses. Additionally, if a continuum equation can be systematically derived from atomistic principles, there is the possibility of discriminating between inherently atomistic effects and those that find a natural expression in a coarse-grained framework. Continuum equations also provide the opportunity for examining the effect of apparently minor modifications to the description of atomistic processes on the coarse-grained evolution of a system which, in turn, facilitates the systematic reduction of full models to their essential components.

3. Methods of multiscale modelling

Each of the methods described in the preceding section is best suited to a particular level of accuracy, as dictated by the successive elimination of the original degrees of freedom. Density function methods provide a quantum mechanical description of electrons and nuclei, which is appropriate for processes such as crack formation, chemical reactions and surface kinetics, where chemical bonds deviate appreciably from their equilibrium configurations and, in extreme cases, such as fracture, break. Where deviations from equilibrium are small but atomistic resolution is still necessary, molecular dynamics offers many computational advantages over a full density functional calculation. Monte Carlo methods are especially useful for obtaining statistical information about a system from the transition rates between configurations, whether in equilibrium or driven away from equilibrium. Finally, continuum equations provide a reduced description in terms of continuous fields for the coarse-grained evolution of the system.

The fundamental tenet of multiscale modelling is that information at each scale is systematically incorporated in a manner that transcends the single-scale description. There are two basic strategies for accomplishing this: sequential and concurrent. In the sequential approach, information from a calculation over particular length and time scales is used as input into a more coarse-grained method. This approach presumes that the phenomenon of interest can be separated into processes that operate at distinct length and time scales. In concurrent multiscale modelling, these disparate scales are combined within a single hybrid scheme, typically involving atomistic and continuum calculations. The main theoretical challenge is to merge the two descriptions in a manner that avoids any spurious effects due this heterogeneity. This approach is well suited to the simulation of fracture, where the complex feedback between the atomic-scale interactions and macroscopic stresses pre-empts a clear-cut separation of scales.

Several methodologies have been implemented within the sequential and concurrent frameworks. In this section we review the main approaches and provide examples of each methodology. Methods of sequential multiscale modelling include sequential parametrization, interface propagation and systematic coarse graining. Concurrent strategies typically combine an atomistic method, such as an *ab initio* density functional calculation or molecular dynamics simulation, with continuum equations that are solved with a finite element method or some other discretization. An introduction to several multiscale methods with worked examples may be found in [29].

3.1. Sequential parametrization

The simplest type of multiscale modelling is sequential parametrization, whereby the output of one calculation is used as input to a more coarse-grained method. In principle, this approach can

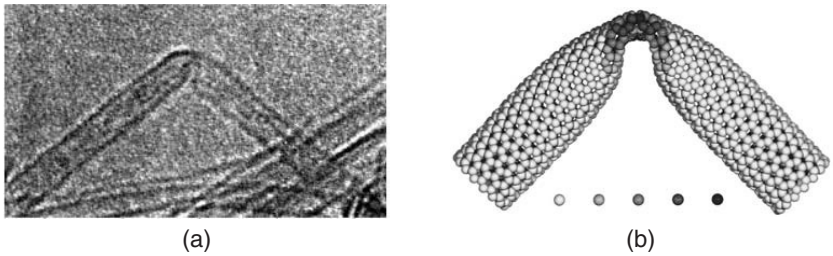

Figure 4. (a) A high-resolution electron microscopy image of a kink structure formed in a single-walled nanotube under mechanical stress [113]. The diameter of the tube is 1.2 nm. (b) The atomic structure of a single kink obtained in a molecular dynamics simulation of the nanotube in (a) [113]. The shading denotes the local strain energy of the atoms measured relative to a relaxed atom in an infinite graphite sheet. The strain energy ranges from 0 to 1.2 eV/atom, from left to right. Reprinted with permission from Sumio Iijima, Charles Brabec, Amitesh Maiti and Jerzy Bernholc 1996 *J. Chem. Phys.* **104** 2089. Copyright 1996, American Institute of Physics.

be used to climb the sequential ladder from *ab initio* to continuum methods. In practice, either density functional or molecular dynamics calculations are used to identify and parametrize processes for kinetic Monte Carlo simulations. Because of the substantial computational resources required, density functional parametrizations of KMC simulations have become feasible only in the past few years [104–108]. The main advantage of this approach is that the consequences of particular atomistic processes can be examined. But these processes must first be identified, usually 'by hand', and their rates calculated, which relies on the accuracy of the calculation. This is especially critical for systems whose characteristics depend on a delicate balance between competing processes [109].

3.1.1. Computational chemistry of liquid water. A noteworthy early example of sequential parametrization was carried out by Clementi and co-workers [110, 111] on liquid water. Beginning with *ab initio* quantum mechanical calculations of water clusters $(H_2O)_n$, for $n = 1, 2, \ldots, 8$, an intermolecular potential was derived with two-, three- and four-body terms (see equation (9)). Although static properties, such as x-ray and neutron scattering intensities, are described quite well by two-body interactions alone, three- and four-body terms are necessary to obtain the enthalpy and other thermodynamic and dynamic properties. The full interatomic potential was then used in a molecular dynamics simulation to obtain sound velocities in liquid water that were in agreement with the available experimental data.

3.1.2. Deformation behaviour of carbon nanotubes. The remarkable mechanical properties of carbon nanotubes are derived from their underlying graphitic network, which is known for its strength and elasticity. Simulations of deformation properties [112–114] have revealed the surprising fact that a nanotube, which has a diameter of the order of a nanometre, can be modelled as a narrow hollow cylinder that follows the laws of *continuum* mechanics. For example, for bending below a sharp critical curvature, the nanotube undergoes compression on the inner side and tension on the outer side (figure 4). This is the regime of Hooke's law, where the strain energy increases quadratically with the bending angle. At a critical angle, strain energy is released through the formation of a kink, after which the strain energy increases linearly with the bending angle. Within the continuum description this behaviour corresponds to a reversible transformation to a different morphological pattern of the nanotube [112]. The atomic structure of nanotubes is manifested directly only for bending angles beyond

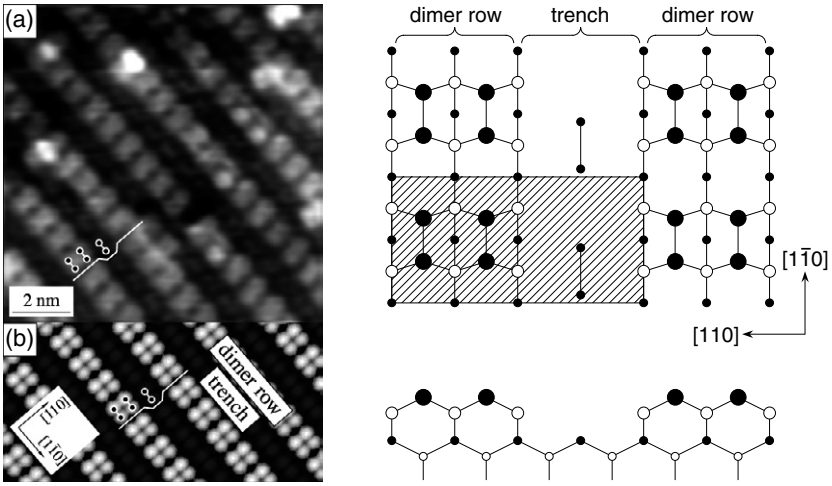

Figure 5. (Left panel.) (a) A filled-state scanning tunnelling microscopy (STM) image of an 11 nm × 11 nm section of the GaAs(001)-$\beta 2(2 \times 4)$ surface. (b) A simulated STM image of the structure in (a) [117]. (Right panel.) Side and plan views of the $\beta 2(2 \times 4)$ reconstruction of GaAs(001), showing alternate rows of dimer pairs and missing-dimer trenches. Filled and open circles represent As and Ga atoms, respectively, with the size indicating their proximity to the surface. The surface unit cell is indicated by the shaded region. Reprinted with permission from V P LaBella, H Yang, D W Bullock, P M Thibado, P Kratzer and M Scheffler 2000 *Phys. Rev. Lett.* **83** 2989. Copyright 2000, American Physical Society.

120°, which results in bond breaking and a damaged nanotube upon unbending in the form of dangling bonds. Although quantum and classical molecular dynamics can be used to model the deformation properties of individual narrow nanotubes [112–114], continuum theory provides a practical alternative for ensembles of nanotubes.

3.1.3. Atomistic growth kinetics during homoepitaxy on GaAs(001). GaAs(001) has been one of the most intensively studied surfaces for the past 30 years due to its importance as a substrate for epitaxial growth. An atomistic description of the growth kinetics on this surface presents a significant modelling challenge, mainly for two reasons: the vastly different surface kinetics of the two incident species (atomic Ga and either As_2 or As_4) and the presence of surface phases ('reconstructions') with complex atomic rearrangements that are determined by the relative fluxes of these species and the substrate temperature. The (2×4) phase occupies the largest region of the temperature-flux 'phase diagram' [115] and is the substrate used for most studies of homoepitaxial growth on this surface. The structure of the most stable of the (2×4) phases, the so-called $\beta 2(2 \times 4)$ reconstruction, has been determined by first-principles density functional calculations [116, 117] which are supported by extensive STM studies [117–119]. This reconstruction, shown in figure 5, is an As-terminated structure that substantially modifies the three topmost atomic layers of the bulk-terminated surface. Alternate pairs of dimer rows along [1$\bar{1}$0], together with their underlying Ga atoms, are missing and the exposed As atoms in the third layer form dimers along this direction.

The Ga and As surface kinetics occur over a vast range of time scales. Adatom hopping on the $\beta 2(2 \times 4)$ phase of GaAs(001) occurs over timescales of microseconds, while island nucleation occurs over timescales of milliseconds or longer. Moreover, even an 'elementary' process, such as adatom hopping, may involve the collective motion of many atoms. The most

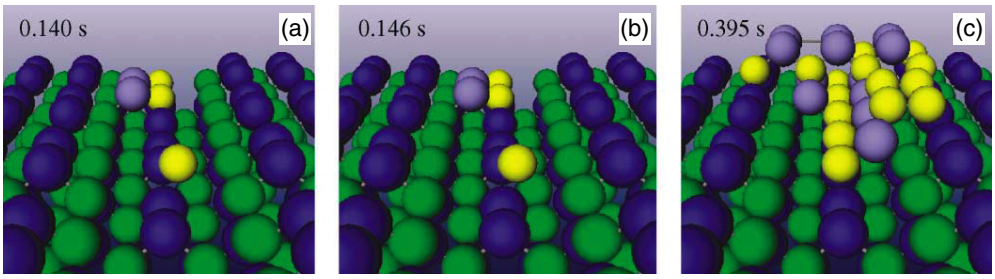

Figure 6. Snapshots from a KMC simulation of homoepitaxy on GaAs(001)-$\beta 2(2 \times 4)$ that has been parametrized by first-principles density functional calculations [123]. The sequence shows ((a), (b)) the filling of the trenches to form a local $\beta(2 \times 4)$ structure and (c) the nucleation of the next layer by the adsorption of As_2 onto a cluster of four Ga atoms. The view is along the $[1\bar{1}0]$ direction (see figure 5). Reprinted with permission from P Kratzer and M Scheffler 2002 *Phys. Rev. Lett.* **88** 036102. Copyright 2002, American Physical Society.

accurate method of describing such complex scenarios is by determining the energetics of the pertinent structures and process using *ab initio* density functional calculations. This facilitates the construction of a potential energy surface [120], the identification of local minima of metastable structures [121] and pathways for processes such as the deposition and incorporation of molecular species [122]. This information can be used to create a database of rates for the kinetic Monte Carlo method for performing simulations over laboratory length and time scales. Such a procedure has been carried out for homoepitaxy on GaAs(001)-$\beta 2(2 \times 4)$ [123]. The energy barriers characterizing the growth sequence deduced from these calculations, together with potential energy surface for Ga adatoms, were used as input to a KMC simulation. The growth sequence is initiated by filling a trench to produce a $\beta(2 \times 4)$ reconstruction locally (figures 6(a), (b)). The next layer is formed by the adsorption of As_2 onto a cluster of four Ga atoms on top of this dimer triplet (figure 6(c)). The completion of the layer then proceeds by the repetition of these steps.

3.1.4. Molecular dynamics and kinetic Monte Carlo simulations of growth kinetics. The first implementation of an atomistic parametrization utilized molecular dynamics simulations based on the Stillinger–Weber potential to study the growth kinetics on Si(001)-(2×1) [124–126]. More recent applications have included a hybrid reformulation of growth on Si(001)-(2×1) [127], embedded-atom parametrizations for simulations of homoepitaxial growth on Cu(001) by molecular beam epitaxy [128, 129] and hyperthermal copper deposition on Cu(111) [130].

3.1.5. Experimental parametrization of kinetic Monte Carlo simulations. An altogether different approach to parametrizing kinetic Monte Carlo simulations is based on the *experimental* determination of the rates of the important atomistic processes, usually from comparisons between simulated and experimental morphologies of growing surfaces. This inevitably involves some degree of iterative optimization to determine the rates of various processes. Examples of this approach are Pt diffusion and aggregation on Pt(111) [131], homoepitaxy on GaAs(001)-$\beta 2(2 \times 4)$ [132, 133] and Ag diffusion on Pt(111) [134].

3.2. Interface propagation

The formation of nanostructures from the assembly of material deposited onto a surface may be viewed as the creation and propagation of heterogeneous interfaces. At this level of abstraction,

the growth of nanostructures is similar to phenomena such as combustion, multiphase fluid flow and solidification, all of which are characterized by fronts that can develop sharp corners and change topologically as they evolve. The characterization of these processes requires methods for following such fronts that capture this complex evolution. In this section, we will describe two approaches to modelling nanostructures in terms of propagating interfaces: the level set method and the phase field method.

3.2.1. The level set method. The central idea of the level set method [135–137] is that any boundary curve Γ can be represented as the set of points $\mathbf{x}$ for which $\phi(\mathbf{x}) = 0$, called the *level set*, for a smooth function ϕ. Given the boundary velocity $\mathbf{v}$, the equation for ϕ is

$$\frac{\partial \phi}{\partial t} + \mathbf{v} \cdot \nabla \phi = 0. \tag{24}$$

The evolution of ϕ, and therefore of Γ, is a consequence of a particular choice of $\mathbf{v}$. An important feature of this method is that ϕ remains smooth throughout any topological changes in Γ, as shown in figure 7 for the nucleation, growth and coalescence of monolayer islands. The solution of equation (24) is obtained numerically with higher-order (typically third-order) accuracy using essentially nonoscillatory methods [138].

The application of the level set method to the morphological evolution of a growing surface necessitates several modifications to the basic foregoing scenario [139, 140]. Multilayer morphologies with boundaries Γ_n on the nth monolayer ($n = 1, 2, \ldots$) are defined as the set of points $\mathbf{x}$ for which $\phi(\mathbf{x}, t) = n$ (figure 7(d)). The velocity is determined by step–adatom interactions and includes processes such as attachment, detachment and edge diffusion. Finally, there is island nucleation, i.e. the *creation* of island boundaries. This involves two steps.

(i) The adatoms are replaced by a continuous density, with the appropriate boundary conditions at step edges, that is updated at each time step. This is a natural and numerically efficient representation that is utilized in several other hybrid atomistic/continuum methods [141–144].
(ii) The nucleation times are chosen from a homogeneous rate equation prescription, but the positions of these events are determined from a probability weighted by the square of the adatom density [145]. This choice produces the correct spatial correlations between islands through the distribution of island sizes.

This discussion illustrates the eminent suitability of the level set method to the modelling of complex processes during nanostructure formation [140, 146] by coupling auxiliary fields to the evolution of ϕ. The adatom density allows the application of the method to homoepitaxial systems, while elastic fields would extend this to strain effects in the heteroepitaxial arena. Co-existing surface reconstructions can also be included by the introduction of separate functions ϕ for each phase [147]. The method has also been extended to dislocation dynamics by describing dislocation lines in three dimensions as the intersection of the level sets of two separate functions [148].

3.2.2. The phase field method. The phase field method provides an alternative mathematical description of free boundary problems for phase transitions, such as solidification and the assembly of structures on a surface, in which the interface has a finite, but small, thickness. The central quantity in this method is an auxiliary function, called the *phase field*, whose value identifies the phase at every point in space and time. The phase field model of the solid–liquid phase transition was first proposed by Langer [149], and has developed into a widely used method for computing realistic growth structures in a variety of settings [150].

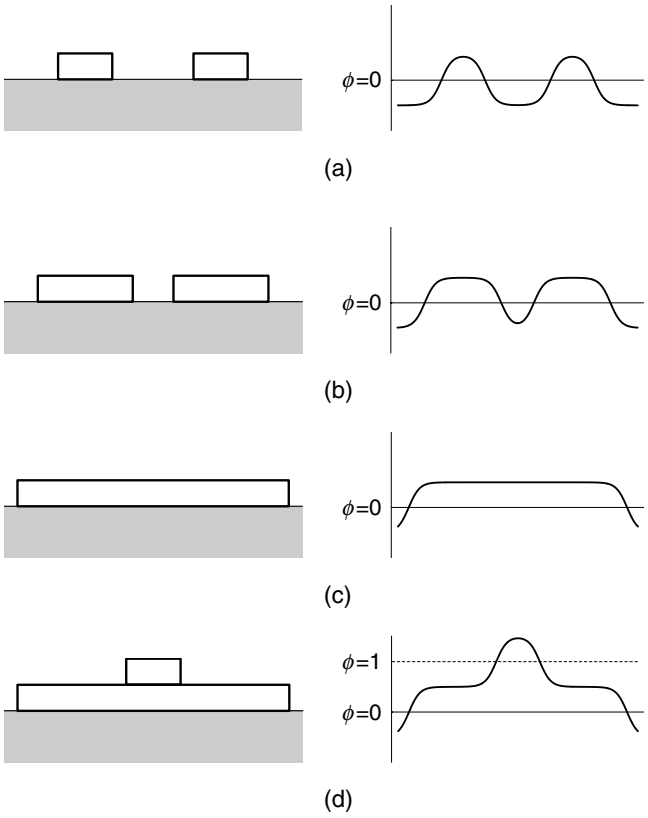

Figure 7. A schematic representation of the level set formalism for the (a) nucleation, (b) growth and (c) coalescence of monolayer islands. Shown are the island morphologies (left) and the level set function ϕ (right) that represents these morphologies. The level set function remains smooth throughout the topological changes of the island morphology. The growth rate of the islands is determined by a particular choice of **v** in equation (24). The morphology in (d) shows the nucleation of a second atomic layer and the modification of the level set function that accommodates this process. (Adapted from figure 1 in [140].)

The phase field φ takes distinct values in different phases, e.g. $\varphi = 0$ in the liquid or vacuum and $\varphi = 1$ in the solid, and changes smoothly, albeit abruptly, between these values across the interface between the two phases. As an example, consider the following equation of motion for φ:

$$\frac{\partial \varphi}{\partial t} = -\frac{\delta F_0}{\delta \varphi}, \tag{25}$$

where

$$F_0 = \int \left[\varphi^2(1-\varphi)^2 + \tfrac{1}{2}\epsilon(\boldsymbol{\nabla}\varphi)^2\right] \mathrm{d}\mathbf{r}. \tag{26}$$

Notice that these terms are nonvanishing only in the interfacial region. Equations (25) and (26) yield the following dynamical equation for φ:

$$\frac{\partial \varphi}{\partial t} = \epsilon^2 \nabla^2 \varphi - 2\frac{\partial[\varphi^2(1-\varphi)^2]}{\partial \varphi}. \tag{27}$$

In one dimension, the stationary solution to this equation is

$$\varphi(r) = \frac{1}{2}\left[1 - \tanh\left(\frac{r}{\epsilon}\right)\right], \tag{28}$$

which identifies ϵ as the width over which the value of φ changes from zero to unity. In the absence of a driving force, the interface remains at rest, with this profile.

Driving forces are incorporated into the phase field formalism by adding appropriate terms to the free energy in equation (26). Consider, for example, the case where the motion of the interface is coupled to elastic stress. For an isotropic solid, the elastic free energy F_e is

$$F_e = \int \left(\tfrac{1}{2}\varepsilon_{ii}^2 + \mu\varepsilon_{ij}^2\right) \mathrm{d}\mathbf{r}, \tag{29}$$

where λ and μ are Lamé coefficients, with μ being the shear modulus. The total free energy F of the system is written as

$$F = F_0 + F_e(\{\varepsilon_{ij}\}, \phi), \tag{30}$$

where μ is replaced by $\mu(\phi) = \mu\phi^2(3 - 2\phi)$, so that $\mu(0) = 0$ and $\mu(1) = \mu$, i.e. the shear modulus is equal to μ in the solid and vanishes in the liquid (or vacuum) [151]. The relaxational equation of motion for ϕ is now written as

$$\frac{\partial\varphi}{\partial t} = -R\frac{\delta F}{\delta\varphi}, \tag{31}$$

where R sets the timescale for the evolution of φ. To complete the mathematical formulation, the equation for the elastic field is obtained from the presumption that the interface dynamics occurs on a faster timescale than sound propagation. This implies that ε_{ij} satisfies the static equation

$$\frac{\delta F}{\delta\varepsilon_{ij}} = 0. \tag{32}$$

Equations (31) and (32) are solved subject to appropriate initial conditions, first for the elastic field and then for the motion of the interface (through ϕ) [151].

The phase field method has been applied to stress-induced instabilities [151], the motion of steps [152–154], island nucleation and growth [155, 156] and self-organized nanostructures [157].

3.3. Hybrid methods

Many physical systems can be spatially decomposed into regions where atomic positions deviate appreciably from equilibrium, requiring a description based on density functional theory or, possibly, molecular dynamics, and those where such deviations are small, for which a continuum description is suitable. Hybrid methods exploit this spatial structure for performing simultaneous atomistic and continuum calculations in appropriate regions of the system; individual implementations differ in how the two calculations are combined. In this section, we describe two basic approaches to hybrid calculations: spatial partitioning and coarse graining.

3.3.1. Spatial partitioning: atomistic and finite element calculations. We illustrate the implementation of this hybrid approach with the scheme proposed by Broughton *et al* [158–161]. The entire system is described in terms of a Hamiltonian whose degrees of freedom are the positions and velocities of the atoms in the atomic region, and the displacements and rates of change of elements in the continuum region. If molecular dynamics is used within the atomic

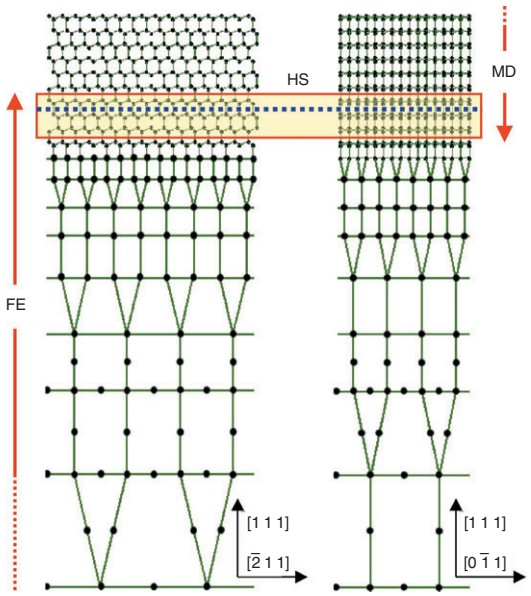

Figure 8. Hybrid scheme for two orientations of a silicon crystal, showing the transition between molecular dynamics (MD) and finite element (FE) regions through 'handshaking' (HS) regions (red box) [162]. The circles within the FE region represent nodes and the elements are bounded by lines. Within the handshaking region the elements and nodes of the FE region merge into the atomic structure of the MD region. Reprinted with permission from E Lidorikis, M E Bachlechner, R K Kalia, A Nakano, P Vashishta and G Z Voyiadjis 2001 *Phys. Rev. Lett.* **87** 086104. Copyright 2001, American Physical Society.

region, the Hamiltonian $\mathcal{H}_{\mathrm{MD}}$ for the atomic degrees of freedom is given by equations (7) and (9):

$$\mathcal{H}_{\mathrm{MD}} = \tfrac{1}{2}\sum_{\alpha}^{N_{\mathrm{a}}} m_\alpha \mathbf{V}_\alpha^2 + \tfrac{1}{2}\sum_{\alpha\neq\beta}^{N_{\mathrm{a}}} U_2(\mathbf{R}_{\alpha\beta}) + \tfrac{1}{6}\sum_{\alpha\neq\beta\neq\gamma}^{N_{\mathrm{a}}} U_3(\mathbf{R}_{\alpha\beta}, \mathbf{R}_{\beta\gamma}, \mathbf{R}_{\beta\gamma}), \tag{33}$$

where N_{a} is the number of atoms in the system and only two- and three-body interaction terms have been included in the interatomic potential. In the continuum region, the relatively small displacements from equilibrium can be described by the equations of linear elasticity, which are solved using the finite element method (section 2.4).

The atomic and continuum descriptions merge at an interface region, wherein the finite elements are fine grained down to the atomic scale (figure 8). This is necessary to enable the finite element region to represent the waves emitted by the molecular dynamics region and thereby minimize any spurious reflections at the interface. Within the interface region, the atomic lattice and finite elements overlap, yielding a one-to-one correspondence between atoms and finite element nodes. The Hamiltonian in this region is defined as the 'average' of the molecular dynamics and finite element Hamiltonians in equations (23) and (33) [160, 161]. The total Hamiltonian $\mathcal{H}$ is therefore written as

$$\begin{aligned}\mathcal{H} = {} & \tfrac{1}{2}\sum_{\alpha}^{N} m_\alpha \mathbf{V}_\alpha^2 + \tfrac{1}{2}\sum_{\alpha\beta}^{N_{\mathrm{a}}} w_{\alpha\beta} U_2(\mathbf{R}_{\alpha\beta}) \\ & + \tfrac{1}{6}\sum_{\alpha\neq\beta\neq\gamma}^{N_{\mathrm{a}}} w_{\alpha\beta\gamma} U_3(\mathbf{R}_{\alpha\beta}, \mathbf{R}_{\alpha\gamma}, \mathbf{R}_{\beta\gamma}) + \tfrac{1}{2}\sum_{ij}^{N_{\mathrm{n}}}\sum_{l}^{N_{\mathrm{e}}} w_l \mathbf{u}_i^l K_{ij}^l \mathbf{u}_j^l,\end{aligned} \tag{34}$$

where N is the total number of particles, with $N < N_a + N_n$ because of the overlap of atoms and nodes in the interface region. The single-body weights w_l are defined as 1 if l lies in the finite element region, $\frac{1}{2}$ if l lies in the interface region and 0 if l lies in the molecular dynamics region. The two-body weights $w_{\alpha\beta}$ and three-body weights $w_{\alpha\beta\gamma}$ are similarly defined [162].

For greater accuracy, a quantum mechanical region can be embedded within the atomic region, which is then coupled to the molecular dynamics region in a manner similar to that in equation (34). The total Hamiltonian may now be written as [161]

$$\begin{aligned}\mathcal{H} = {} & \mathcal{H}_{\mathrm{QM}}(\{\mathbf{r}_i, \dot{\mathbf{r}}_i, \mathbf{R}_\alpha, \dot{\mathbf{R}}_\alpha\}) + \mathcal{H}_{\mathrm{QM/MD}}(\{\mathbf{r}_i, \dot{\mathbf{r}}_i, \mathbf{R}_\alpha, \dot{\mathbf{R}}_\alpha\}) \\ & + \mathcal{H}_{\mathrm{MD}}(\{\mathbf{R}_\alpha, \dot{\mathbf{R}}_\alpha\}) + \mathcal{H}_{\mathrm{MD/FE}}(\{\mathbf{R}_\alpha, \dot{\mathbf{R}}_\alpha, \mathbf{u}_i, \dot{\mathbf{u}}_i\}) \\ & + \mathcal{H}_{\mathrm{FE}}(\{\mathbf{u}_i, \dot{\mathbf{u}}_i\}),\end{aligned} \tag{35}$$

in which the notation signifies that there are separate Hamiltonians for the quantum mechanical (QM), molecular dynamics (MD) and finite element (FE) regions, as well as Hamiltonians for each of the two interface regions, denoted by QM/MD and MD/FE. The equations of motion of all the variables are obtained by taking the appropriate derivatives of $\mathcal{H}$ and, for a given set of initial conditions, the system evolves in a manner that conserves the total energy. Although the spatial decomposition is well suited to parallel computation, the integration of the equations of motion is based on a single time step for the entire system, so the issue of disparate timescales is not addressed directly.

3.4. Coarse graining of atomistic degrees of freedom

The spatial partitioning of a system into atomistic and continuum regions requires a 'handshaking' interface between the two descriptions. Quite apart from spurious effects that may arise from this construction, the position of the interface is determined by balancing computational resources against numerical accuracy. An altogether different approach is a gradual transition between the atomistic and continuum regions in which their coupling is derived from the underlying atomistic interactions through coarse graining. The atomistic degrees of freedom are retained where deviations from equilibrium are appreciable, e.g. near a defect, but are replaced by a coarser description in regions where the spatial variation of the system is small. In this section, we describe three methods that implement this strategy: the quasicontinuum method, the coarse-grained molecular dynamics approach and coarse-grained kinetic Monte Carlo simulations.

3.4.1. The quasicontinuum method. The quasicontinuum method [163–165] is based on standard finite elements and constitutive equations derived from atomistic interactions. There are two main ingredients of this method:

(1) Finite elements on a mesh refined to the atomistic level in critical regions near a defect, such as the core of a dislocation, but coarsened in regions where the variation of the displacement is small (figure 9). These regions can evolve during the deformation.

(2) The selection of a subset from the N atoms in the system of N_r 'representative atoms', in terms of which the displacements of all the atoms can be expressed. The total energy is computed only from the representative atoms using, for example, the Cauchy–Born rule, which calculates the local energy by assuming that the deformation is locally uniform. In the atomistic region, all of the atoms are representative atoms, while, in the coarse-grained region, the density of representative atoms is substantially reduced, so $N_r \ll N$ (figure 9).

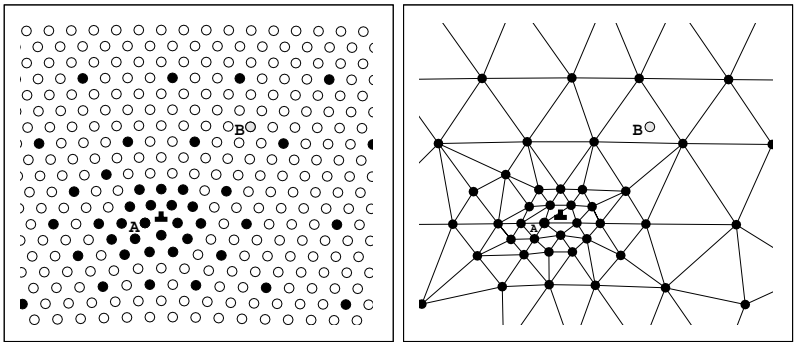

Figure 9. (a) The selection of representative atoms (indicated by dark circles) in the neighbourhood of a dislocation [164]. Near the dislocation core, in the vicinity of atom A, where deformation gradients are large, all atoms are representative. Where deformation gradients are comparatively small, atom B can represent the deformation of several atoms in its vicinity. (b) The finite element grid constructed from the representative atoms in (a). With kind permission of Springer Science and Business Media.

Given the positions of all N atoms in the system, the total potential energy can be written in terms of their displacements $\mathbf{u}_i$ from equilibrium as

$$E = E(\mathbf{u}_1, \mathbf{u}_2, \ldots, \mathbf{u}_\mathrm{N}), \tag{36}$$

i.e. as a function of all the displacements. If there is an external load applied to the system, producing a force $\mathbf{f}_i$ on atom i, the quantity $-\sum_{i=1}^{N} \mathbf{f}_i \cdot \mathbf{u}_i$ is added to equation (36). The first step of the quasicontinuum method is to express the displacements of all atoms in terms of the displacements $\mathbf{u}_\alpha (\alpha = 1, \ldots, N_\mathrm{r})$ of the representative atoms from the shape functions in equation (22):

$$\tilde{\mathbf{u}}_i = \sum_{\alpha=1}^{N_\mathrm{r}} \varphi_\alpha(\mathbf{r}_{0,i})\mathbf{u}_\alpha, \tag{37}$$

where $\mathbf{r}_{0,i}$ is the undeformed position of the ith atom and the tilde indicates that the displacements are interpolated, rather than exact, values. The representative atoms are the nodes of the finite element mesh. The energy of the system becomes

$$E = E(\tilde{\mathbf{u}}_1, \tilde{\mathbf{u}}_2, \ldots, \tilde{\mathbf{u}}_\mathrm{N}). \tag{38}$$

The calculation of this energy, although based on the exact displacements only of the representative atoms, still involves all of the N atoms in the system.

The total energy is now written as the sum of energies associated with each atom individually:

$$E = \sum_{i=1}^{N} E_i(\tilde{\mathbf{u}}_1, \tilde{\mathbf{u}}_2, \ldots, \tilde{\mathbf{u}}_\mathrm{N}). \tag{39}$$

This decomposition occurs naturally for molecular dynamics Hamiltonians, as in equation (34), but not for the density functional Hamiltonian in equations (2) and (3). This expression is now approximated by summing only over the representative atoms, with weighting factors to account for the differences in element size and environment:

$$E_\mathrm{r} = \sum_{\alpha=1}^{N_\mathrm{r}} n_\alpha E_\alpha, \tag{40}$$

where n_α is the number of atoms subsumed by the representative atom α.

The evaluation of E_r can be obtained by invoking the Cauchy–Born principle, resulting in what is known as the *local* version of the quasicontinuum method. The use of linear functions φ_α in equation (37) to interpolate the displacement field implies that the deformation gradient $\mathbf{F} = \partial\mathbf{u}/\partial\mathbf{r}$ (see equation (18)) is uniform within each element. The Cauchy–Born principle stipulates that a uniform deformation at the macroscopic scale can be mapped onto the same deformation at the atomistic scale. For crystalline solids with simple lattice structures, this implies that all atoms in a region of uniform deformation gradient are energetically equivalent. Thus, the energy of an element is obtained from the product of the energy of *any* atom in that element and the number of atoms contained within the element. The energy in equation (40) accordingly reduces to

$$E_r = \sum_{j=1}^{N_e} \Omega_j \mathcal{E}(\mathbf{F}_j), \tag{41}$$

where Ω_j is the volume of the jth element and $\mathcal{E}$ is the energy density for a deformation gradient of $\mathbf{F}_j$. The summation implicit in equation (36) over the atoms in the system has been thereby reduced to a sum over elements.

The local quasicontinuum method provides a considerable computational simplification of the evaluation of the total energy in equation (36) and, where surface and interface energetics are unimportant, a reasonable approximation to the energetics of the system. But there are several important situations where these assumptions cannot be justified, including dislocation cores (atom A in figure 9), multiatom unit cells and phase boundaries. For such circumstances, a *nonlocal* version of the quasicontinuum method has been developed, based on the ansatz where the total energy of the system can be written as

$$E = \sum_{\alpha=1}^{N_r} n_\alpha E_\alpha(\mathbf{u}_\alpha). \tag{42}$$

The energy E_α of each representative atom is calculated from the deformed neighbouring environment determined by the interpolated displacements within the elements. The main advantage of the nonlocal quasicontinuum method is that its atom-refined limit corresponds exactly to molecular statics, which thus correctly describes the structures of dislocation cores and interfaces such as stacking faults and grain boundaries.

The basic form of the quasicontinuum method just described is confined to zero-temperature static equilibrium, wherein lattice vibrations are neglected and dynamical and inertial effects during deformation are deemed unimportant. Attempts at extending the method to incorporate such effects have included zero-temperature dynamics based on classical equations of motion [166] and coarse graining by integrating the partition function over atoms not explicitly chosen as representative atoms [166, 167].

3.4.2. Coarse-grained molecular dynamics. The coarse graining of molecular dynamics [168, 169] is similar in philosophy to the quasicontinuum method. The basic idea is to obtain a coarse-grained set of finite element equations from an atomistic molecular dynamics Hamiltonian, as in equation (33). In the following, we denote atomic positions with Greek indices and finite element nodes with Latin indices. Thus, the displacement of atom α from its equilibrium position is $\mathbf{u}_\alpha$. The nodal displacements $\mathbf{u}_j$ and momenta $\mathbf{p}_j$ of the finite element mesh are weighted averages of the corresponding atomic quantities:

$$\mathbf{u}_j = \sum_\alpha f_{j\alpha}\mathbf{u}_\alpha, \qquad \mathbf{p}_j = \sum_\alpha f_{j\alpha}\mathbf{p}_\alpha, \tag{43}$$

where $f_{j\alpha}$ is obtained from the finite element interpolating function in equation (22) in a manner to be described below. Since the number of atoms is greater than or equal to the

number of nodes, specifying nodal displacements and velocities does not determine all of the corresponding atomic quantities. The coarse-grained energy is defined as the classical canonical ensemble average of the molecular dynamics Hamiltonian $\mathcal{H}_{\mathrm{MD}}$:

$$E(\{\mathbf{u}_k\},\{\mathbf{p}_k\}) = \frac{1}{\mathcal{Z}}\int\cdots\int\prod_{\alpha}\mathrm{d}x_\alpha\,\mathrm{d}p_\alpha\,\Delta\mathcal{H}_{\mathrm{MD}}\mathrm{e}^{-\beta\mathcal{H}_{\mathrm{MD}}}, \tag{44}$$

in which $\beta = 1/(k_{\mathrm{B}}T)$ and T is the absolute temperature, $\mathcal{Z}$ is the partition function and Δ enforces the constraints for the displacements and velocities in equation (43):

$$\Delta = \prod_j \delta\left(\mathbf{u}_j - \sum_\alpha f_{j\alpha}\mathbf{u}_\alpha\right)\delta\left(\mathbf{p}_j - \sum_\alpha f_{j\alpha}\mathbf{p}_\alpha\right). \tag{45}$$

Equations (43) and (44) are the central equations of coarse-grained molecular dynamics. The final step in the formulation is determining $f_{j\alpha}$. For a given set of atomic displacements $\mathbf{u}_\alpha$, the finite element representation of the displacement field in equation (22) yields

$$u(\mathbf{r}_\alpha) = \sum_{j=1}^{N_{\mathrm{n}}}\mathbf{u}_j\varphi_j(\mathbf{r}_\alpha) \equiv \sum_{j=1}^{N_{\mathrm{n}}}\mathbf{u}_j\varphi_{j\alpha}. \tag{46}$$

Requiring the $\mathbf{u}_j$ in equation (43) to produce the best least squares fit to the atomic displacements,

$$\chi^2 = \sum_\alpha |\mathbf{u}_\alpha - \mathbf{u}(\mathbf{r}_\alpha)|^2 = \sum_\alpha\left|\mathbf{u}_\alpha - \sum_j \mathbf{u}_j\varphi_{j\alpha}\right|^2, \tag{47}$$

yields

$$f_{j\alpha} = \sum_k\left(\sum_\beta \varphi_{j\beta}\varphi_{k\beta}\right)^{-1}\varphi_{k\alpha}, \tag{48}$$

where the inverse is a matrix inverse. For a one-dimensional chain with harmonic springs and an incommensurate mesh, the error in the phonon spectrum obtained with coarse-grained molecular dynamics is less than 6% compared with the exact result, while that obtained with the finite element method exceeds 18% [168].

When the mesh nodes and the atomic sites are identical, $f_{j\alpha} = \delta_{j\alpha}$, and the coarse-grained equations of motion are the same as those obtained from the molecular dynamics Hamiltonian (equation (7)). This limit illustrates an important difference from the conventional finite element method, namely, that the basic equations of the coarse-grained methodology are atomistic equations of motion, rather than partial differential equations that are discretized on the nodes of the mesh. As the mesh size increases, shorter-wavelength modes are eliminated by the coarse-graining process and their effect on the remaining modes is included indirectly through the thermodynamic average in equation (44). This description is expected to be valid, provided that the system is initially in thermodynamic equilibrium and changes to the short-wavelength modes are adiabatic. The remaining modes are under no such restrictions and may thereby be driven out of equilibrium at will.

3.4.3. Coarse-grained kinetic Monte Carlo simulations. The atomistic assembly of surface nanostructures can be viewed as particles on a lattice that interact according to a set of prescribed rules for processes such as deposition, surface diffusion and desorption. Kinetic Monte Carlo simulations of such systems have provided the basis of much of our understanding of the morphological consequences of particular atomistic processes [170–173]. Continuum descriptions embody a more global view of morphological evolution, which is especially

important for heteroepitaxial growth in the presence of misfit strain [174–176], where nonlocal elastic interactions have hindered the widespread application of KMC simulations [177]. In this section we describe a systematic coarse-graining method for deriving continuum equations from the transition rules on a lattice.

In principle, such methods begin at the atomic scale and produce descriptions at the mesoscale and finally a coarse-grained equation for the macroscopic degrees of freedom. Renormalization group methods developed initially for static and dynamical critical phenomena have been applied to molecular dynamics [167] and lattice growth models [197], and wavelet-based methods have been developed for lattice systems [198–200]. In this section we describe a method for coarse graining lattice models of the morphological evolution of interfaces.

We consider a one-dimensional model with only random deposition and surface diffusion to demonstrate the elements of the coarse-graining methodology; the procedure for higher-dimensional models is essentially the same, but with correspondingly greater computational overheads. The system is a lattice of length L on every site i of which is a column of height h_i. Every surface configuration $\mathbf{H}$ is specified completely by the array $\mathbf{H} = \{h_1, h_2, \ldots, h_L\}$. The probability $P(\mathbf{H}, t)$ of the system having configuration $\mathbf{H}$ at time t is a solution of the master equation [93],

$$\frac{\partial P}{\partial t} = \sum_{\mathbf{r}} [W(\mathbf{H} - \mathbf{r}; \mathbf{r}) P(\mathbf{H} - \mathbf{r}, t) - W(\mathbf{H}; \mathbf{r}) P(\mathbf{H}, t)], \tag{49}$$

where $W(\mathbf{H}; \mathbf{r})$ is the transition rate from $\mathbf{H}$ to $\mathbf{H} + \mathbf{r}$, $\mathbf{r} = \{r_1, r_2, \ldots\}$ is the array of all jump lengths r_i and the summation over $\mathbf{r}$ is the joint summation over all the r_i.

The solution of the master equation is obtained by invoking a limit theorem due to Kurtz [178–180], which states that, provided that the intrinsic fluctuations are not too large, the solution of equation (49) is asymptotically equivalent to that of the Langevin equations

$$\frac{\mathrm{d}h_i}{\mathrm{d}t} = K_i^{(1)}(\mathbf{H}) + \eta_i, \tag{50}$$

where the η_i are Gaussian noises that have a zero mean, $\langle \eta_i(t) \rangle = 0$, and covariance

$$\langle \eta_i(t) \eta_j(t') \rangle = K_{ij}^{(2)}(\mathbf{H}) \delta(t - t'), \tag{51}$$

where the first and second moments of the transition rates are given by

$$K_i^{(1)}(\mathbf{H}) = \int r_i W(\mathbf{H}; \mathbf{r}) \, \mathrm{d}\mathbf{r}, \tag{52}$$

$$K_{ij}^{(2)}(\mathbf{H}) = \int r_i r_j W(\mathbf{H}; \mathbf{r}) \, \mathrm{d}\mathbf{r}. \tag{53}$$

For random deposition, the configurations $\mathbf{H}$ and $\mathbf{H} + \mathbf{r}$ differ by the addition of a single particle to a randomly chosen column. The associated transition rate is

$$W(\mathbf{H}; \mathbf{r}) = \tau^{-1} \sum_i \delta_{r_i,1} \prod_{j \neq i} \delta_{r_j,0}, \tag{54}$$

where τ^{-1} is the deposition rate. The transition rate for the hopping of a particle from site i to site j is

$$W(\mathbf{H}; \mathbf{r}) = \sum_{ij} w_{ij} \delta_{r_i,-1} \delta_{r_j,1} \prod_{k \neq i,j} \delta_{r_k,0}, \tag{55}$$

where the hopping rate and hopping rules are contained in the w_{ij}. Surface diffusion is often modelled as nearest neighbour hopping, with Arrhenius rates based on the number of nearest neighbours of the initial state, in which case we have

$$w_{ij} = \tfrac{1}{2} \Gamma_i (\delta_{i,j-1} + \delta_{i,j+1}), \tag{56}$$

where $\Gamma_i = k_0 e^{-\beta E_i}$, $k_0 \sim 10^{13}$ s^{-1} is the attempt frequency, $\beta = 1/k_B T$ and E_i is the energy barrier for hopping from the ith site. A common choice is $E_i = E_S + n_i E_N$, where E_S is a site independent barrier due to the substrate, E_N is the contribution from each lateral nearest neighbour and n_i is the number of such neighbours.

With the total transition rate given by the sum of equations (54) and (55), the first and second moments of this quantity are [181]

$$K_i^{(1)} = \tfrac{1}{2}\Delta^2 K_i + \tau^{-1}, \tag{57}$$

$$K_{ij}^{(2)} = \tfrac{1}{2}\left[\delta_{ij}\Delta^2\Gamma_i - (\Gamma_i + \Gamma_j)\Delta^2\delta_{ij}\right] + \delta_{ij}\tau^{-1}, \tag{58}$$

in which the discrete second difference $\Delta^2 f_i = f_{i-1} - 2f_i + f_{i+1}$ acts only on the first index of δ_{ij}. The counting of nearest neighbours is carried out with step functions, whose singular behaviour necessitates a careful regularization to obtain a sensible continuum limit [181]. One such scheme [182, 183] has recently been applied to two other standard models of deposition: the Edwards–Wilkinson and Wolf–Villain models. For the model at hand, this yields a smoothed lattice equation of motion from which the renormalization group flow is toward the fixed point of the equation proposed by Villain [184] and by Lai and Das Sarma [185]:

$$\frac{\partial h}{\partial t} = -\nu\frac{\partial^4 h}{\partial x^4} - \lambda\frac{\partial^2}{\partial x^2}\left(\frac{\partial h}{\partial x}\right)^2 + \xi \tag{59}$$

where $\nu > 0$, $\lambda > 0$ and the ξ have mean zero and covariance

$$\langle \eta_i(x,t)\eta_j(x',t')\rangle = \tau^{-1}\delta(x-x')\delta(t-t'). \tag{60}$$

Although focusing on the fixed point prevents a direct connection between the coefficients ν and λ and the hopping rates in equation (56), such a connection *can* be made in the crossover regime, as has been demonstrated for the Wolf–Villain model [183]. Comparisons between the morphological evolution of epitaxial surfaces with solutions of equation (59) and other proposed equations have been used to estimate the magnitudes and *signs* of the coefficients, thereby inferring the influence of particular processes [186, 187].

4. A case study: self-organized quantum dots

Semiconductor quantum dots offer the promise of many technological and scientific innovations, ranging from optoelectronics [188, 189] to quantum computing [190]. All of these applications are based on the confinement of carriers within quantum dots to discrete energy levels, as well as a degree of spatial self-organization. The practical implementation of heterostructures based on quantum dots relies on the uniformity of their sizes to ensure, for example, that a large number of dots are active at a specified optical wavelength.

The basic principle behind the formation of quantum dots is the formation of coherent three-dimensional (3D) islands during the Stranski–Krastanov growth of a highly strained system [191, 192]. The prototypical cases are InAs on GaAs(001) (7% lattice misfit) and Ge on Si(001) (4% lattice misfit). When the islands are embedded within a material with a wider band gap, the carriers within the islands are confined by the potential barriers that surround each island, thereby forming an array of quantum dots. Because these quantum dots are obtained directly by growth, with no additional processing, they are referred to as *self-organized* or *self-assembled* structures.

Although quantum dots are routinely produced in laboratories throughout the world, many fundamental questions remain about the self-organization process. The 3D islands are formed through a nucleation process, but unless the substrate is prepared with preferential nucleation sites (e.g. through patterning [193] or dislocation networks [194]), the ensemble of islands

exhibits a distribution of volumes that leads to a far greater inhomogeneous broadening than is acceptable for optical applications.

The challenges for modelling stem from the fact that the self-organization of quantum dot arrays is an inherently multiscale phenomenon. We consider the InAs/GaAs system as an example. The nucleation process is known to favour a specific reconstruction and surface orientation: the c(4 × 4) phase of GaAs(001) (figure 3(a)). The dots form abruptly and with varying degrees of spatial correlation (figure 3(c)). As they grow, the increasing strain energy suppresses the attachment of migrating adatoms, which promotes self-limiting growth. The calculation of electronic states within quantum dots requires detailed information on their size and shape (figure 3(b)); the absence of such information has meant that the available calculations have provided only semi-quantitative information. The strain field associated with quantum dots affects the nucleation of three-dimensional islands in subsequent layers, which promotes vertical self-organization of quantum dot arrays (figure 3(d)). In this section we review the multiscale modelling studies that have addressed the formation of self-organized quantum dots.

4.1. First-principles studies of InAs/GaAs(001) heteroepitaxy

First-principles calculations provide detailed information about specific materials systems. For nanostructure formation and other supported kinetic processes this includes the stability of surface reconstructions, potential energy surfaces for the diffusion of surface atoms and energy barriers for other processes, which can be used in KMC simulations (see section 3.1.3), and the effect of strain on these barriers. Such calculations have been carried out for the initial stages of quantum dot formation in the InAs/GaAs system, such as the surface phase diagram of GaAs(001) [116, 201, 202], InAs(001) [36, 203], including alloy phases, and the effect of strain on these phases as a function of the As chemical potential [36, 204], potential energy surfaces for In and Ga adatom migration on the GaAs substrate and for models for the InGaAs wetting layer [205].

The investigation of In migration on GaAs(001)-c(4 × 4) can provide insight into the initial stages of the wetting layer formation, and analogous studies on the $In_{2/3}Ga_{1/3}As$ alloy surface can provide insight into adatom migration on the wetting layer(s), despite not necessarily corresponding to the actual structure of the wetting layer. First-principles calculations [36, 206] reveal that the corrugation of the potential energy surface for In migration on $In_{2/3}Ga_{1/3}As$ is remarkably small, showing a maximum variation of $\simeq$0.5 eV, which is markedly less than that for GaAs(001)-c(4 × 4). The highly mobile In (and Ga) adatom population is thereby poised to respond to any changes in the surface chemical potential brought about by the nucleation of islands. This is leads to an initially rapid island nucleation rate, which is a characteristic signature of these systems [207, 208].

Indium migration on GaAs(001)-c(4 × 4) is significantly affected by strain and shows a linear dependence for small strains [209, 210]. For an inhomogeneously strained sample, this implies a position dependent activation energy for In migration. By using a flat island on this surface, Kratzer *et al* [213] have shown that strain leads to a repulsive potential with a strength of up to 0.2 eV that affects both the binding energy and, to a somewhat smaller extent, the diffusion barriers for an In adatom that approaches such an island (figure 10). This repulsion can severely impede the growth rate of strained islands and has been cited [211, 212] as a key factor for narrowing the island-size distribution. A simulation [205] of two elongated islands that compete for In adatoms does indeed show that the sizes of the growing islands tend to equalize.

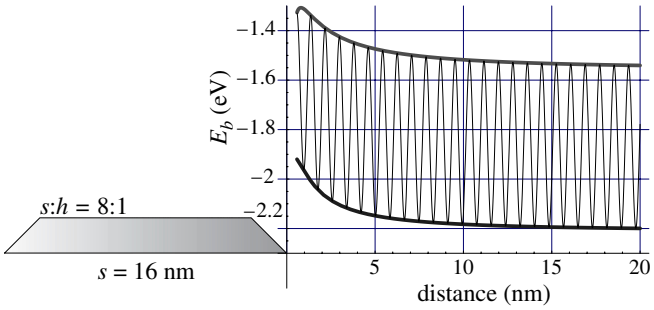

Figure 10. The migration potential (right panel) for an In adatom near a coherent InAs island (of width s and height h) on GaAs(001)-c(4 × 4) [36]. In addition to the diffusion potential due to the atomic structure of the surface, the strain field in the substrate caused by the island produces a repulsive potential that lifts both the binding energies (lower bold curve) and transition state energies (upper bold curve) near the island.

4.2. Hybrid molecular dynamics–finite element calculation of strain in nanopixels

The effects of strain on the ordered self-assembly of quantum dot ensembles originate with the interplay between the elastic energy within individual dots and the elastic interaction between dots. The strain within each dot affects its composition, shape and growth rate. Interactions between dots are evident in vertical self-organization (figure 3(d)), whereby the strain field of buried dots creates preferential nucleation sites for the next layer of quantum dots [195]. A description of such self-organization kinetics requires a calculation that consolidates the short-range atomistic and long-range continuum manifestations of strain.

Such a calculation, with the hybrid molecular dynamics/finite element method described in section 3.3.1, has been reported by Lidorikis *et al* [162], albeit on a Si/Si_3N_4 nanopixel on Si(111), rather than a quantum dot. The geometry is shown in figure 11. In the molecular dynamics region, the Stillinger–Weber potential [71] was used for Si, a combination of two- and three-body terms (see equation (9)) for Si_3N_4 that include electronic polarizability, charge transfer and covalent bonding, and a variation of this potential for the Si/Si_3N_4 interface to account for the charge transfer and bonding determined from electronic structure calculations.

The absolute displacements of this system are shown in figure 11. A comparison is shown between a full molecular dynamics simulation and the hybrid calculation to demonstrate the effectiveness of the hybrid methodology in reproducing the details of molecular dynamics. Appreciable displacements are seen well below the handshaking region, an important effect for the vertical self-organization of quantum dot ensembles. A separate calculation with the handshaking region placed 30 Å below the surface of the substrate produced essentially identical results. The application of this hybrid scheme, or indeed any modelling that utilizes molecular dynamics for the InAs/GaAs system, necessitates first developing adequate interaction potentials for this complex system. Su *et al* [196] have reported large-scale molecular dynamics simulations of InAs/GaAs square nanomesas which, insofar as such comparisons are meaningful, are consistent with the results in figure 11.

4.3. Off-lattice kinetic Monte Carlo simulations of Stranski–Krastanov growth

As discussed in section 3.3, current implementations of hybrid strategies address the presence of multiple *spatial* scales, but not multiple time scales. The simulation of heteroepitaxial kinetic phenomena, which typically have competing strain relaxation mechanisms [216, 217],

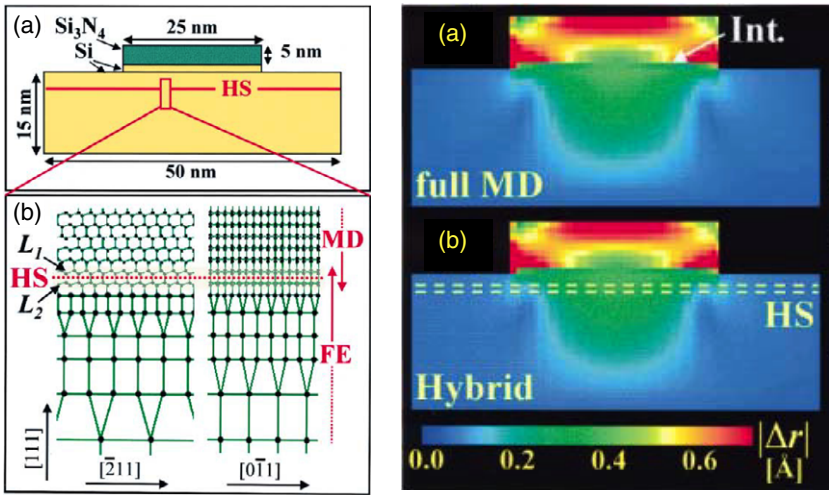

Figure 11. (Left.) (a) Two-dimensional projection of the Si/Si_3N_4 nanopixel, with Si and Si_3N_4 shown green and yellow, respectively. (b) The handshaking (HS) region separating the molecular dynamics (MD) and finite element (FE) regions in the Si substrate along two directions. This region lies 10 Å below the surface of the substrate. The circles within the FE region represent nodes and the elements are bounded by lines (see figure 8) [162]. (Right.) Absolute displacement $|\Delta r|$ from equilibrium within a slice through the centre of the pixel for (a) a full molecular dynamics simulation and (b) the hybrid molecular dynamics–finite element calculation [162]. Reprinted with permission from E Lidorikis, M E Bachlechner, R K Kalia, A Nakano, P Vashishta and G Z Voyiadjis 2001 *Phys. Rev. Lett.* **87** 086104. Copyright 2001, American Physical Society.

has thereby relied upon kinetic Monte Carlo simulations based on simplified structures and rules for particular systems. Lattice-based simulations [177] are appropriate for coherent (i.e. dislocation-free) morphologies, but the continuous atomic positions in off-lattice models [214, 215] allow deviations from a perfect lattice structure that are dictated by an interatomic potential, including the possibility of dislocation formation. KMC simulations of off-lattice models, where transition rates are calculated directly from an interatomic potential, provide a temporal coarse-graining approximation to a full molecular dynamics simulation, which would be impractical for the typical time scales of quantum dot formation, even with modern acceleration strategies [86].

Biehl *et al* [218, 219] have carried out off-lattice KMC simulations on one-dimensional substrates using a Lennard-Jones potential,

$$U_{\alpha\beta} = 4U_0 \left[\left(\frac{\sigma}{R_{\alpha\beta}} \right)^{12} - \left(\frac{\sigma}{R_{\alpha\beta}} \right)^{6} \right], \tag{61}$$

where the distance $R_{\alpha\beta} = |\mathbf{R}_\alpha - \mathbf{R}_\beta|$ between atoms α and β is a continuous variable. The simulation proceeds by assigning an Arrhenius rate to each transition event i,

$$r_i = \nu_0 \exp(-E_i/k_B T), \tag{62}$$

where ν_0 is the attempt frequency and E_i is the energy barrier for the process. These simulations are particularly simple for one-dimensional substrates because the path between neighbouring local minima of the potential energy is uniquely determined, and the transition state corresponds to the separating local maximum.

The interactions within the two different materials in the simulation, the substrate and the adsorbate, are characterized by the parameters (U_s, σ_s) and (U_a, σ_a), respectively, in

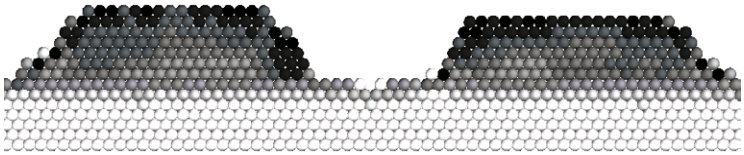

Figure 12. A section of a simulated crystal obtained for a flux of 7.0 ML s^{-1} and a simulation temperature $T = 500$ K [219]. Islands are located on a wetting layer of approximately one monolayer thickness and the six bottom layers represent the substrate. The darker the shading of a particle, the larger the average distance from its nearest neighbours. The parameters used were $U_s = 1.0$ eV, $U_a = 0.74$ eV, $U_{as} \approx 0.86$ eV.

equation (61), and substrate–adsorbate interactions by

$$U_{as} = \sqrt{U_s U_a}, \qquad \sigma_{as} = \tfrac{1}{2}(\sigma_s + \sigma_a). \tag{63}$$

Since the lattice constant of a monatomic Lennard-Jones crystal is proportional to σ, the relative misfit is given by $\epsilon = (\sigma_a - \sigma_s)/\sigma_s$. For the simulation of SK growth, the parameters were chosen such that $\sigma_a > \sigma_s$, with $\epsilon = 4\%$, and $U_s > U_{as} > U_a$.

A typical morphology is shown in figure 12. The substrate is flat prior to the onset of deposition, and growth proceeds initially in a layer-by-layer manner, as the wetting layers are formed. At a well-defined thickness, monolayer islands on the wetting layer undergo a rapid transition to bilayer islands. This suggests that the emergence of islands upon islands, i.e. the transition to three-dimensional growth, is due mainly to upward particle hops onto existing monolayer islands. After this transition, islands grow by incorporating material from the deposition flux as well as that from the surrounding wetting layer. Atoms near the centre of three-dimensional islands adopt positions close to the minimum of the nearest potential energy trough, while atoms further from the centre of the island are correspondingly further away from their nearest minima (figure 12). Thus, strain relaxation occurs predominantly at the edges of islands, as expected.

4.4. Nonlinear evolution equation for self-organization

Continuum equations enable the consequences of elastic interactions for the self-organization of quantum dots to be identified, while providing a framework for the atomistic origins of this morphology to be explored. The basic mathematical requirement of such a theory [176] is that the morphological instability that leads to the formation of islands in finite time must saturate, leading to islands of finite size. We consider a theory [174–176] in which an epitaxial thin film wets a rigid substrate. The evolution equation for the height h of this film is

$$\frac{\partial h}{\partial t} = \mathcal{D}\sqrt{1 + |\nabla h|^2}\nabla_S^2(\mathcal{E} + \gamma\mathcal{K} + \Phi), \tag{64}$$

in which $\mathcal{D}$ is proportional to the surface diffusivity, $\mathcal{E}(h)$ is the elastic energy [175], γ is the surface energy and $\mathcal{K}$ is the curvature of the surface, and Φ is the wetting chemical potential, which is a function of the film thickness, local slope and curvature: $\Phi = \Phi(h, |\nabla h|^2, \nabla^2 h)$.

The linear stability analysis [174] of this model (without Φ) indicates that there is a critical thickness below which the film is stable and above which it is unstable. Moreover, the wavenumbers of perturbations corresponding to instability just above the critical thickness are small. Thus, the nonlinear evolution of the film can be described using a small-slope approximation. This has the virtue of transforming the free boundary elastic problem into an evolution equation for the free surface. The small-slope approximation of equation (64) can

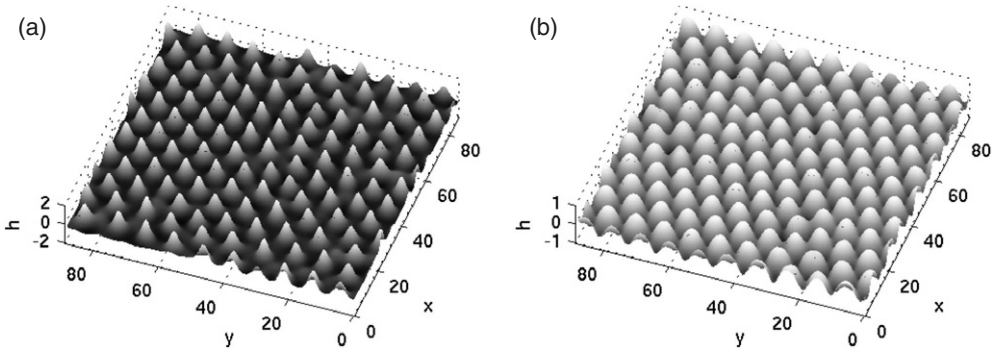

Figure 13. Quantum dot morphologies obtained from the numerical solution of equation (65) for particular choices of the parameters g, p and q: (a) a hexagonal array of cone-type dots obtained for $g = 0.2$, $p = 2$ and $q = -0.5$ and (b) a hexagonal array of cap-type dots, obtained for $g = 0.01$, $p = -4$, and $q = 1$ [176]. Reprinted with permission for A A Golovin, S H Davis and P W Voorhees, 2003 *Phys. Rev.* E **68** 056203. Copyright 2003, American Physical Society.

be written as [176]

$$\frac{\partial h}{\partial t} = g\nabla^2 h + \nabla^4 h + \nabla^6 h + \nabla^2\left[h\nabla^2 h + p(\nabla h)^2 + qh^2\right], \tag{65}$$

where g, p and q are adjustable constants given in terms of the elastic constants of the film and model parameters. The linear stability of this equation can be assessed for a perturbation of the form $h \sim e^{\sigma t + i\mathbf{k}\cdot\mathbf{r}}$, which yields the dispersion relation $\sigma = -gk^2 + k^4 - k^6$. The instability is seen for $g < g_c = \frac{1}{4}$ at a wavenumber of $k_c = \frac{1}{2}\sqrt{2}$. This nonzero critical value of k_c, which is a direct result of the wetting layer contribution to the elastic energy, is responsible for the emergence of solutions of equation (65) with stationary periodic patterns (figure 13).

Although equation (65) was not initially developed as a multiscale theory, such a point of view would be of evident benefit here. Solutions of this equation do indeed produce a variety of morphologies for different values of g, p and q, but the appropriate values for any particular system are not easily determined, and the relationship to underlying atomistic processes is not at all clear, which pre-empts a direct calculation of these parameters. On the other hand, the equation of motion for h in equation (65) is of the form one would expect to emerge from the coarse graining of atomistic models discussed in section 3.4.3. Indeed, such an analysis [220] of the model used by Ratsch *et al* [177] for the onset of three-dimensional islanding does yield most of the terms in equation (65). Once a direct connection to atomistic processes can be established, a first-principles approach can be applied to determine the appropriate growth morphology for particular systems as a function of their growth conditions.

5. Summary and outlook

We have surveyed the current status of multiscale modelling, beginning with density functional theory, molecular dynamics, Monte Carlo simulations and continuum mechanics. These methods, which form the basic elements of virtually all implementations of multiscale strategies, were initially developed independently as specialized techniques. Multiscale modelling synthesizes these atomistic and continuum methods to provide a more natural and coherent description of materials phenomena than that obtained from the fragmented perspective of a limited range of length and time scales. But the multiscale paradigm is not

without its limitations. The three main challenges facing future development of multiscale modelling are:

- *Simulations at finite temperatures.* Many of the methods we have described are confined to zero temperature, wherein the basic quantity is a Hamiltonian for the system expressed in terms of the appropriate degrees of freedom. In principle, Hamiltonian methods can be extended to equilibrium at finite temperatures by using the free energy, but inherently nonequilibrium situations are fundamentally different and a general approach is not close at hand.
- *Time scales accessible by means of molecular dynamics.* The bottleneck for macroscopic time simulations remains the small time step used in classical and quantum molecular dynamics. While this may be side-stepped in certain applications (e.g. section 4.3), and acceleration strategies are available for particular situations [86], a general acceleration methodology would have revolutionary implications that would stretch across many disciplines.
- *Mode transmission across atomistic/continuum interfaces.* In methods with a sharp interface between atomistically resolved and (finite element) continuum regions, high-frequency modes emanating from the molecular region must be accommodated by the continuum region. However, the finite elements are unable to resolve the small wavelengths of the atomistic region and, since such multiscale methods are based typically on a Hamiltonian formulation, which means that energy is conserved, the modes are reflected back into the atomistic region, which can lead to spurious results.

Despite these imposing technical challenges, multiscale methods are poised to unravel the secrets of nanostructures and other materials that will transform science and technology in the coming century.

Acknowledgments

This review is based on a series of lectures presented at the UCLA Institute of Pure and Applied Mathematics (IPAM) programme on *Mathematics in Nanoscale Science and Engineering* in September 2002. The author is grateful to the staff of IPAM for their hospitality and to all the participants for their input, but special thanks go to Russ Caflisch, Petr Plechac and Christian Ratsch for many helpful discussions. The support of the Engineering and Physical Sciences Research Council is also gratefully acknowledged.

References

[1] Feynman R P 1960 There's plenty of room at the bottom—an invitation to enter a new field of physics *Eng. Sci. (Caltech)* **23** 22 (http://www.zyvex.com/nanotech/feynman.html)
[2] Eigler D M and Schweitzer E K 1990 Positioning single atoms with a scanning tunneling microscope *Nature* **344** 524–6
[3] Stroscio J A and Eigler D M 1991 Atomic and molecular manipulation with the scanning tunneling microscope *Science* **254** 1319–26
[4] Moriarty J A, Belak J F, Rudd R E, Soderlind P, Streitz F H and Yang L H 2002 Quantum-based atomistic simulation of materials properties in transition metals *J. Phys.: Condens. Matter* **14** 2825–57
[5] Moriarty J A, Vitek V, Bulatov V V and Yip S 2002 Atomistic simulations of dislocations and defects *J. Comput.-Aided Mater.* **9** 99–132
[6] Lu G, Zhang Q, Kioussis N and Kaxiras E 2001 Hydrogen-enhanced local plasticity in aluminum: an *ab initio* study *Phys. Rev. Lett.* **87** 095501
[7] Cuitino A M 1997 A time-dependent deformation mechanism in metallic fcc crystals *Acta Mater.* **45** 2509–22

[8] Cuitino A M, Stainier L, Wang G F, Strachan A, Cagin T, Goddard W A and Ortiz M 2002 A multiscale approach for modelling crystalline solids *J. Comput.-Aided Mater.* **8** 127–49

[9] Holian B L 2003 Formulating mesodynamics for polycrystalline materials *Europhys. Lett.* **64** 330–6

[10] Moore G E 1965 Cramming more components onto integrated circuits *Electronics* **38** 114–7

[11] Hutcheson G D 2004 The first nanochips *Sci. Am.* **290** 48–55

[12] Zhirnov V V, Cavin R K III, Hutchby J A and Bourianoff G I 2003 Limits to binary logic switch scaling—a Gedanken model *Proc. IEEE* **91** 1934–9

[13] http://www.intel.com

[14] http://public.itrs.net

[15] Iijima S 1991 Helical microtubes of graphitic carbon *Nature* **354** 56–8

[16] Treacy M M J, Ebbesen T W and Gibson J M 1996 Exceptionally high Young's modulus observed for individual carbon nanotubes *Nature* **381** 678–80

[17] Wong E W, Sheehan P E and Lieber C M 1997 Nanobeam mechanics: elasticity, strength, and toughness of nanorods and nanotubes *Science* **277** 1971–5

[18] Gao H and Kong Y 2004 Simulation of DNA–nanotube interactions *Annu. Rev. Mater. Res.* **34** 123–50

[19] Suenaga K, Tencé M, Mory C, Colliex C, Kato H, Okazaki T, Shinohara H, Hirahara K, Bandow S and Iijima S 2000 Element-selective single atom imaging *Science* **290** 2280–2

[20] Kasemo B 2002 Biological surface science *Surf. Sci.* **500** 656–77

[21] Nakano A, Bachlechner M E, Kalia R K, Lidorikis E, Vashishta P, Voyiadjis G Z, Campbell T J, Ogata S and Shimojo F 2001 Multiscale simulation of nanosystems *Comput. Sci. Eng.* **3** 56–66

[22] Kubin L P, Bassani J L, Cho K, Gao H and Selinger R L B (ed) 2001 *Multiscale Modeling of Materials* (*Materials Research Society Symp. Proc.* vol 653) (Pittsburgh, PA: Materials Research Society)

[23] Bulatov V, Cleri F, Colombo L, Lewis L and Mousseau N (ed) 2002 *Advances in Materials Theory and Modeling—Bridging Over Multiple-Length and Time Scales* (*Materials Research Society Symp. Proc.* vol 677) (Pittsburgh, PA: Materials Research Society)

[24] Guo Z X, Pettifor D, Kubin L and Kostorz G (ed) 2003 *1st Int. Conf. on Multiscale Materials Modelling*; *Mater. Sci. Eng.* A **365** 1–354

[25] Nieminen R M 2002 From atomistic simulation towards multiscale modelling of materials *J. Phys.: Condens. Matter* **14** 2859–76

[26] Curtin W A and Miller R E 2003 Atomistic/continuum coupling in computational materials science *Modelling Simul. Mater. Sci. Eng.* **11** R33–68

[27] Ghoniem N M, Busso E P, Kioussis N and Huang H 2003 Multiscale modelling of nanomechanics and micromechanics: an overview *Phil. Mag.* **83** 3457–528

[28] Liu W K, Karpov E G, Zhang S and Park H S 2004 An introduction to computational nanomechanics and materials *Comput. Methods Appl. Mech. Eng.* **193** 1529–78

[29] Park H S and Liu W K 2004 An introduction and tutorial on multiple-scale analysis in solids *Comput. Methods Appl. Mech. Eng.* **193** 1733–72

[30] Diaz de la Rubia T and Bulatov V V (ed) 2001 Materials research by means of multiscale computer simulation *Mater. Res. Soc. Bull.* **26** 169–221

[31] King P R 1987 The use of field theoretic methods for the study of flow in a heterogeneous porous medium *J. Phys. A: Math. Gen.* **20** 3935–47

[32] King P R and Neuweiler I 2002 Probability upscaling *Comput. Geosci.* **6** 101–14

[33] Spohn H 1991 *Large-Scale Dynamics of Interacting Particles* (Berlin: Springer)

[34] Liggett T 1999 *Stochastic Interacting Systems: Contact, Voter, and Exclusion Processes* (New York: Springer)

[35] Blanc X, Le Bris C and Lions P-L 2002 From molecular models to continuum mechanics *Arch. Ration. Mech. Anal.* **164** 341–81

[36] Penev E and Kratzer P 2004 First-principles study of InAs/GaAs(001) heteroepitaxy *Quantum Dots: Fundamentals, Applications, Frontiers* ed B A Joyce, P C Kelires, A G Naumovets and D D Vvedensky (Dordrecht: Kluwer) pp 27–42

[37] Nagashima A, Tazima M, Nishimura A, Takagi Y and Yoshino J 2001 Structural analysis of GaAs(001)-c(4×4) with LEED IV technique *Surf. Sci.* **493** 227–31

[38] Jacobi K 2003 Atomic structure of InAs quantum dots on GaAs *Prog. Surf. Sci.* **71** 185–215

[39] Goldman R S 2004 Nanoprobing of semiconductor heterointerfaces: Quantum dots, alloys and diffusion *J. Phys. D: Appl. Phys.* **37** R163–78

[40] Hohenberg P and Kohn W 1964 Inhomogeneous electron gas *Phys. Rev.* **136** B864–71

[41] Kohn W and Sham L J 1965 Self-consistent equations including exchange and correlation effects *Phys. Rev.* **140** A1133–8

[42] Levy M 1979 Universal variational functionals of electron densities, first-order density matrices, and natural spin–orbitals and solution of the v-representability problem *Proc. Natl Acad. Sci. USA* **76** 6062–5
[43] Ceperley D M and Alder B J 1980 Ground state of the electron gas by a stochastic method *Phys. Rev. Lett.* **45** 566–9
[44] Gunnarsson O, Jonson M and Lundqvist B I 1979 Descriptions of exchange and correlation effects in inhomogeneous electron systems *Phys. Rev.* B **20** 3136–64
[45] Jones R O and Gunnarsson O 1989 The density functional formalism, its applications and prospects *Rev. Mod. Phys.* **61** 689–746
[46] Hood R Q, Chou M Y, Williamson A J, Rajagopal G, Needs R J and Foulkes W M C 1997 Quantum Monte Carlo investigation of exchange and correlation in silicon *Phys. Rev. Lett.* **78** 3350–3
[47] Hood R Q, Chou M Y, Williamson A J, Rajagopal G and Needs R J 1998 Exchange and correlation in silicon *Phys. Rev.* B **57** 8972–82
[48] Langreth D C and Perdew J P 1980 Theory of nonuniform electronic systems: I. Analysis of the gradient approximation and a generalization that works *Phys. Rev.* B **21** 5469–93
[49] Langreth D C and Mehl M J 1983 Beyond the local-density approximation in calculations of ground-state electronic properties *Phys. Rev.* B **28** 1809–34
[50] Perdew J P and Wang Y 1986 Accurate and simple density functional for the electronic exchange energy: generalized gradient approximation *Phys. Rev.* B **33** 8800–2
[51] Perdew J P, Burke K and Ernzerhof M 1996 Generalized gradient approximation made simple *Phys. Rev. Lett.* **77** 3865–8
[52] Car R and Parrinello M 1985 Unified approach for molecular dynamics and density-functional theory *Phys. Rev. Lett.* **55** 2471–4
[53] Payne M C, Teter M P, Allan D C, Arias T A and Joannopoulos J D 1992 Iterative minimisation techniques for *ab initio* total-energy calculations: molecular dynamics and conjugate gradients *Rev. Mod. Phys.* **64** 1045–97
[54] Kurth S, Perdew J P and Blaha P 1999 Molecular and solid-state tests of density functional approximations: LSD, GGAs, and meta-GGAs *Int. J. Quantum Chem.* **75** 889–909
[55] Kohn W 1999 Nobel lecture: electronic structure of matter-wavefunctions and density functionals *Rev. Mod. Phys.* **71** 1253–66
[56] Goedecker S 1999 Linear scaling electronic structure methods *Rev. Mod. Phys.* **71** 1085–123
[57] Soler J M, Artacho E, Gale J D, García A, Junquera J, Ordejón P and Sánchez-Portal D 2002 The SIESTA method for *ab initio* order-N materials simulation *J. Phys.: Condens. Matter* **14** 2745–79
[58] Bowler D R, Miyazaki T and Gillan M J 2002 Recent progress in linear scaling *ab initio* electronic structure techniques *J. Phys.: Condens. Matter* **14** 2781–98
[59] Allen M P and Tildesley D J 1987 *Computer Simulations of Liquids* (Oxford: Oxford University Press)
[60] Haile J M 1992 *Molecular Dynamics Simulation* (New York: Wiley)
[61] Rapaport D C 1995 *The Art of Molecular Dynamics Simulation* (Cambridge: Cambridge University Press)
[62] Verlet L 1967 Computer 'experiments' on classical fluids: I. Thermodynamical properties of Lennard-Jones molecules *Phys. Rev.* **159** 98–103
[63] Verlet L 1968 Computer 'experiments' on classical fluids: II. Equilibrium correlation functions *Phys. Rev.* **165** 201–14
[64] Gear C W 1971 *Numerical Initial Value Problems in Ordinary Differential Equations* (Englewood Cliffs, NJ: Prentice-Hall)
[65] Plimpton S 1995 Fast parallel algorithms for short-range molecular dynamics *J. Comput. Phys.* **117** 1–19
[66] Vashishta P, Bachlechner M, Nakano A, Campbell T J, Kalia R K, Kodiyalam S, Ogata S, Shimojo F and Walsh P 2001 Multimillion atom simulation of materials on parallel computers—nanopixel, interfacial fracture, nanoindentation, and oxidation *Appl. Surf. Sci.* **182** 258–64
[67] Ogata S, Campbell T J, Kalia R K, Nakano A, Vashishta P and Vemparala S 2003 Scalable and portable implementation of the fast multipole method on parallel computers *Comput. Phys. Commun.* **153** 445–61
[68] Jones J E 1924 On the determination of molecular fields: II. From the equation of state of a gas *Proc. R. Soc.* A **106** 463–77
[69] Morse P M 1929 Diatomic molecules according to the wave mechanics: II. Vibrational levels *Phys. Rev.* **34** 57–64
[70] Carlsson A E 1990 Beyond pair potentials for transition-metals and semiconductors *Solid State Physics: Advances in Research and Applications* vol 43, ed H Ehrenreich and D Turnbull (New York: Academic) pp 1–91

[71] Stillinger F H and Weber T A 1985 Computer simulation of local order in condensed phases of silicon *Phys. Rev.* B **31** 5262–71
[72] Tersoff J 1986 New empirical model for the structural properties of silicon *Phys. Rev. Lett.* **56** 632–5
[73] Tersoff J 1988 New empirical approach for the structure and energy of covalent systems *Phys. Rev.* B **37** 6991–7000
[74] Brenner D W 1990 Empirical potential for hydrocarbons for use in simulating the chemical vapor deposition of diamond films *Phys. Rev.* B **42** 9458–71
[75] Daw M S and Baskes M I 1983 Semiempirical, quantum mechanical calculation of hydrogen embrittlement in metals *Phys. Rev. Lett.* **50** 1285–8
[76] Daw M S and Baskes M I 1984 Embedded-atom method: derivation and application to impurities, surfaces, and other defects in metals *Phys. Rev.* B **29** 6443–53
[77] Jacobsen K W, Nørskov J K and Puska M J 1987 Interatomic interactions in the effective-medium theory *Phys. Rev.* B **35** 7423–42
[78] Finnis M W and Sinclair J E 1984 A simple empirical N-body potential for transition metals *Phil. Mag.* A **50** 45–55
[79] Cohen R E, Mehl M J and Papaconstantopoulos D A 1994 Tight-binding total-energy method for transition and noble metals *Phys. Rev.* B **50** 14694–7
[80] Mehl M J and Papaconstantopoulos D A 1996 Applications of a tight-binding total-energy method for transition and noble metals: elastic constants, vacancies, and surfaces of monatomic metals *Phys. Rev.* B **54** 4519–30
[81] Pettifor D G 1989 New many-body potential for the bond order *Phys. Rev. Lett.* **63** 2480–3
[82] Pettifor D G, Finnis M W, Nguyen-Manh D, Murdick D A, Zhou X W and Wadley H N G 2004 Analytic bond order potentials for multicomponent systems *Mater. Sci. Eng.* A **365** 2–13
[83] Moriarty J A 1988 Density-functional formulation of the generalized pseudopotential theory: III. Transition-metal interatomic potentials *Phys. Rev.* B **38** 3199–231
[84] Schneider M, Rahman A and Schuller I K 1985 *Phys. Rev. Lett.* **55** 604–6
[85] Schneider M, Schuller I K and Rahman A 1987 *Phys. Rev.* B **36** 1340–3
[86] Voter A F, Montalenti F and Germann T C 2002 Extending the time scales in atomistic simulation of materials *Annu. Rev. Mater. Res.* **32** 321–46
[87] Landau D and Binder K 2000 *A Guide to Monte Carlo Simulations in Statistical Physics* (Cambridge: Cambridge University Press)
[88] McCracken D D 1955 The Monte Carlo method *Sci. Am.* **192** 90–5
[89] Metropolis N, Rosenbluth A W, Rosenbluth M N, Teller A H and Teller E 1953 Equation of state calculations by fast computing machines *J. Chem. Phys.* **21** 1087–92
[90] Bhanot G 1988 The Metropolis algorithm *Rep. Prog. Phys.* **51** 429–57
[91] Kang H C and Weinberg W H 1989 Dynamic Monte Carlo with a proper energy barrier: surface diffusion and two-dimensional domain ordering *J. Chem. Phys.* **90** 2824–30
[92] Fichthorn K A and Weinberg W H 1991 Theoretical foundations of dynamical Monte Carlo simulations *J. Chem. Phys.* **95** 1090–6
[93] Van Kampen N G 1981 *Stochastic Processes in Physics and Chemistry* (Amsterdam: North-Holland)
[94] Zangwill A 1988 *Physics at Surfaces* (Cambridge: Cambridge University Press)
[95] Wang Z and Seebauer E G 2001 Estimating pre-exponential factors for desorption from semiconductors: consequences for *a priori* process modelling *Appl. Surf. Sci.* **181** 111–20
[96] Bortz A B, Kalos M H and Lebowitz J L 1975 A new algorithm for Monte Carlo simulation of Ising spin systems *J. Comput. Phys.* **17** 10–8
[97] Maksym P A 1988 Fast Monte Carlo simulations of MBE growth *Semicond. Sci. Technol.* **3** 594–6
[98] Blue J L, Beichl I and Sullivan F 1995 Faster Monte Carlo simulations *Phys. Rev.* E **51** R867–8
[99] Haider N, Khaddaj S A, Wilby M R and Vvedensky D D 1995 Parallel Monte Carlo simulations of epitaxial growth *Comput. Phys.* **9** 85–96
[100] Korniss G, Novotny M A and Rikvold P A 1999 Parallelization of a dynamic Monte Carlo algorithm: a partially rejection-free conservative approach *J. Comput. Phys.* **153** 488–508
[101] Batchelor G K 1967 *An Introduction to Fluid Dynamics* (Cambridge: Cambridge University Press)
[102] Reddy J N 1993 *An Introduction to the Finite Element Method* (New York: McGraw-Hill)
[103] Morton K W and Mayers D F 1994 *Numerical Solution of Partial Differential Equations* (Cambridge: Cambridge University Press)
[104] Smith A P and Jónsson H 1996 Dimer and string formation during low temperature silicon deposition on Si(100) *Phys. Rev. Lett.* **77** 1326–9

[105] Huang H, Gilmer G H and Diaz de la Rubia T 1998 An atomistic simulator for thin film deposition in three dimensions *J. Appl. Phys.* **84** 3636–49
[106] Jónsson H 2000 Theoretical studies of atomic scale processes relevant to crystal growth *Annu. Rev. Phys. Chem.* **51** 623–53
[107] Grosse F, Barvosa-Carter W, Zinck J, Wheeler M and Gyure M F 2002 Arsenic flux dependence of island nucleation on InAs(001) *Phys. Rev. Lett.* **89** 116102
[108] Grosse F and Gyure M F 2002 *Ab initio* based modeling of III–V semiconductor surfaces: thermodynamic equilibrium and growth kinetics on atomic scales *Phys. Rev.* B **66** 075320
[109] Smith A, Wiggs J, Jónsson H, Yan H, Corrales L R, Nachtigall P and Jordan K 1995 Si adatom binding and diffusion on the Si(100) surface: comparison of *ab initio*, semi-empirical and empirical potential results *J. Chem. Phys.* **102** 1044–56
[110] Clementi E 1985 *Ab initio* computational chemistry *J. Phys. Chem.* **89** 4426–36
[111] Clementi E 1988 Global scientific and engineering simulations on scalar, vector and parallel LCAP-type supercomputers *Phil. Trans. R. Soc.* A **326** 445–70
[112] Yakobson B I, Brabec C J and Bernholc J 1996 Nanomechanics of carbon tubes: Instabilities beyond linear response *Phys. Rev. Lett.* **76** 2511–4
[113] Iijima S, Brabec C, Maiti A and Bernholc J 1996 Structural flexibility of carbon nanotubes *J. Chem. Phys.* **104** 2089–92
[114] Bernholc J, Brenner D, Nardelli M B, Meunier V and Roland C 2002 Mechanical and electrical properties of nanotubes *Annu. Rev. Mater. Res.* **32** 347–75
[115] Däweritz L and Hey R 1990 Reconstruction and defect structure of vicinal GaAs(001) and $Al_xGa_{1-x}As(001)$ surfaces during MBE growth *Surf. Sci.* **236** 15–22
[116] Northrup J E and Froyen S 1994 Structure of GaAs(001) surfaces: the role of electrostatic interactions *Phys. Rev.* B **50** 2015–8
[117] LaBella V P, Yang H, Bullock D W, Thibado P M, Kratzer P and Scheffler M 2000 Atomic structure of the GaAs(001)-(2 × 4) surface resolved using scanning tunneling microscopy and first-principles theory *Phys. Rev. Lett.* **83** 2989–92
[118] Hashizume T, Xue Q K, Zhou J, Ichimiya A and Sakurai T 1994 Structures of As-rich GaAs(001)-(2 × 4) reconstructions *Phys. Rev. Lett.* **73** 2208–11
[119] Avery A R, Goringe C M, Holmes D M, Sudijono J L and Jones T S 1996 Mechanism for disorder on GaAs(001)-(2 × 4) surfaces *Phys. Rev. Lett.* **76** 3344–7
[120] Kley A, Ruggerone P and Scheffler M 1997 Novel diffusion mechanism on the GaAs(001) surface: the role of adatom–dimer interaction *Phys. Rev. Lett.* **79** 5278–81
[121] Kratzer P, Morgan C G and Scheffler M 1999 Model for nucleation in GaAs homoepitaxy derived from first principles *Phys. Rev.* B **59** 15246–52
[122] Morgan C G, Kratzer P and Scheffler M 1999 Arsenic dimer dynamics during MBE growth: theoretical evidence for a novel chemisorption state of As_2 molecules on GaAs surfaces *Phys. Rev. Lett.* **82** 4886–9
[123] Kratzer P and Scheffler M 2002 Reaction-limited island nucleation in molecular beam epitaxy of compound semiconductors *Phys. Rev. Lett.* **88** 036102
[124] Zhang Z Y, Lu Y T and Metiu H 1991 Adsorption and diffusion sites of a Si adatom on a reconstructed Si(100)-(2 × 1) surface *Surf. Sci.* **248** L250–4
[125] Lu Y T, Zhang Z Y and Metiu H 1991 The migration of a Si atom adsorbed on the Si(100)-(2 × 1) surface *Surf. Sci.* **257** 199–209
[126] Zhang Z Y and Metiu H 1993 The self-organization of Si atoms adsorbed on a Si(100) surface: an atomic level kinetic model *Surf. Sci.* **292** L781–5
[127] Tavazza F, Nurminen L, Landau D P, Kuronen A and Kaski K 2004 Hybrid Monte Carlo–molecular dynamics algorithm for the study of islands and step edges on semiconductor surfaces: application to Si/Si(001) *Phys. Rev.* E **70** 036701
[128] Biham O, Furman I, Karimi M, Vidali G, Kennett R and Zeng H 1998 Models for diffusion and island growth in metal monolayers *Surf. Sci.* **400** 29–43
[129] Furman I, Biham O, Zuo J K, Swan A K and Wendelken J F 2000 Epitaxial growth of Cu on Cu(001): experiments and simulations *Phys. Rev.* B **62** R10649–52
[130] Pomeroy J M, Jacobsen J, Hill C C, Cooper B H and Sethna J P 2002 Kinetic Monte Carlo–molecular dynamics investigations of hyperthermal copper deposition on Cu(111) *Phys. Rev.* B **66** 235412
[131] Bott M, Hohage M, Morgenstern M, Michely T and Comsa G 1996 New approach for determination of diffusion parameters of adatoms *Phys. Rev. Lett.* **76** 1304–7

[132] Itoh M, Bell G R, Avery A R, Jones T S, Joyce B A and Vvedensky D D 1998 Stable and unstable islands during homoepitaxy on GaAs(001) *Phys. Rev. Lett.* **81** 633–6
[133] Itoh M, Bell G R, Joyce B A and Vvedensky D D 2000 Structural transformation kinetics of epitaxial islands on GaAs(001) *Surf. Sci.* **464** 200–10
[134] Brune H, Bales G S, Jacobsen J, Boragno C and Kern K 1999 Measuring surface diffusion from nucleation island densities *Phys. Rev.* B **60** 5991–6006
[135] Osher S and Sethian J A 1988 Fronts propagating with curvature-dependent speed: algorithms based on Hamilton–Jacobi formulations *J. Comput. Phys.* **79** 12–49
[136] Sethian J A 1999 *Level Set Methods and Fast Marching Methods* (Cambridge: Cambridge University Press)
[137] Osher S J and Fedkiw R P 2002 *Level Set Methods and Dynamic Implicit Surfaces* (New York: Springer)
[138] Osher S and Shu C-W 1991 High-order essentially nonoscillatory schemes for Hamilton–Jacobi equations *SIAM J. Numer. Anal.* **28** 907–22
[139] Chopp D L 2000 A level-set method for simulating island coarsening *J. Comput. Phys.* **162** 104–22
[140] Ratsch C, Gyure M F, Caflisch R E, Gibou F, Petersen M, Kang M, Garcia J and Vvedensky D D 2002 Level-set method for island dynamics in epitaxial growth *Phys. Rev.* B **65** 195403
[141] Mandreoli L, Neugebauer J, Kunert R and Schöll E 2003 Adatom density kinetic Monte Carlo: a hybrid approach to perform epitaxial growth simulations *Phys. Rev.* B **68** 155429
[142] Schulze T P, Smereka P and Weinan E 2003 Coupling kinetic Monte Carlo and continuum models with application to epitaxial growth *J. Comput. Phys.* **189** 197–211
[143] Gill S P A, Spencer P E and Cocks A C F 2004 A hybrid continuum kinetic Monte Carlo model for surface diffusion *Mater. Sci. Eng.* A **365** 66–72
[144] Russo G, Sander L M and Smereka P 2004 Quasicontinuum Monte Carlo: a method for surface growth simulations *Phys. Rev.* B **69** 121406
[145] Ratsch C, Gyure M F, Chen S, Kang M and Vvedensky D D 2000 Fluctuations and scaling in aggregation phenomena *Phys. Rev.* B **61** 10598–601
[146] Baumann F H, Chopp D L, Diaz de la Rubia T, Gilmer G H, Greene J E, Huang H, Kodambaka S, O'Sullivan P and Petrov I 2001 Multiscale modeling of thin-film deposition: applications to Si device processing *Mater. Res. Soc. Bull.* **26** 182–9
[147] Ratsch C, Anderson C, Caflisch R E, Feigenbaum L, Shaevitz D, Sheffler M and Tiee C 2003 Multiple domain dynamics simulated with coupled level sets *Appl. Math. Lett.* **16** 1165–70
[148] Xiang Y, Cheng L-T, Srolovitz D J and E W 2003 A level set method for dislocation dynamics *Acta Mater.* **51** 5499–518
[149] Langer J S 1986 Models of pattern formation in first-order phase transitions *Directions in Condensed Matter Physics* ed G Grinstein and G Mazenko (Philadelphia, PA: World Scientific) pp 164–86
[150] Sekerka R F 2004 Morphology: from sharp interface to phase field models *J. Cryst. Growth* **264** 530–40
[151] Kassner K, Misbah C, Müller J, Kohlert P and Kappey J 2001 Phase-field modeling of stress-induced instabilities *Phys. Rev.* E **63** 036117
[152] Liu F and Metiu H 1994 Stability and kinetics of step motion on crystal surfaces *Phys. Rev.* E **49** 2601–16
[153] Karma A and Plapp M 1998 Spiral surface growth without desorption *Phys. Rev. Lett.* **81** 4444–7
[154] Rätz A and Voigt A 2004 Various phase-field approximations for epitaxial growth *J. Cryst. Growth* **266** 278–82
[155] Castro M 2003 Phase-field approach to heterogeneous nucleation *Phys. Rev.* B **67** 035412
[156] Yu Y-M and Liu B-G 2004 Phase-field model of island growth in epitaxy *Phys. Rev.* E **69** 021601
[157] Kim D and Lu W 2004 Self-organized nanostructures in multi-phase epilayers *Nanotechnology* **15** 667–74
[158] Mullins M and Dokainish M A 1982 Simulation of the (001) plane crack in α-Fe employing a new boundary scheme *Phil. Mag.* A **46** 771–87
[159] Kohlhoff S, Gumbsch P and Fischmeister H F 1991 Crack propagation in bcc crystals studied with a combined finite element and atomistic model *Phil. Mag.* A **64** 851–78
[160] Abraham F F, Broughton J Q, Bernstein N and Kaxiras E 1998 Spanning the length scales in dynamic simulation *Comput. Phys.* **12** 538–46
[161] Broughton J Q, Abraham F F, Bernstein N and Kaxiras E 1999 Concurrent coupling of length scales: methodology and application *Phys. Rev.* B **60** 2391–403
[162] Lidorikis E, Bachlechner M E, Kalia R K, Nakano A, Vashishta P and Voyiadjis G Z 2001 Coupling length scales for multiscale atomistics–continuum simulations: atomistically induced stress distributions in Si/Si_3N_4 nanopixels *Phys. Rev. Lett.* **87** 086104
[163] Tadmor E B, Ortiz M and Phillips R 1996 Quasicontinuum analysis of defects in solids *Phil. Mag.* A **73** 1529–63
[164] Miller R E and Tadmor E B 2002 The quasicontinuum method: overview, applications and current directions *J. Comput.-Aided Mater.* **9** 203–39

[165] http://www.qcmethod.com
[166] Shenoy V, Shenoy V and Phillips R 1999 Finite temperature quasicontinuum methods *Multiscale Modelling of Materials* (*Materials Research Society Symp. Proc.* vol 538) ed V V Bulatov, T Diaz de la Rubia, R Phillips, E Kaxiras and N Ghoniem (Pittsburgh, PA: Materials Research Society) pp 465–71
[167] Curtarolo S and Ceder G 2002 Dynamics of an inhomogeneously coarse grained multiscale system *Phys. Rev. Lett.* **88** 255504
[168] Rudd R E and Broughton J Q 1998 Coarse-grained molecular dynamics and the atomic limit of finite elements *Phys. Rev.* B **58** R5893–6
[169] Rudd R E and Broughton J Q 2000 Concurrent coupling of length scales in solid state systems *Phys. Status Solidi* **217** 251–91
[170] Weeks J D and Gilmer G H 1979 Dynamics of crystal growth *Adv. Chem. Phys.* **40** 157–228
[171] Madhukar A and Ghaisas S V 1988 The nature of molecular beam epitaxial growth examined via computer simulations *CRC Crit. Rev. Solid State Mater. Sci.* **14** 1–130
[172] Shitara T, Vvedensky D D, Wilby M R, Zhang J, Neave J H and Joyce B A 1992 Step-density variations and reflection high-energy electron diffraction intensity oscillations during epitaxial growth on vicinal GaAs(001) *Phys. Rev.* B **46** 6815–24
[173] Metiu H, Lu Y-T and Zhang Z Y 1992 Epitaxial growth and the art of computer simulations *Science* **255** 1088–92
[174] Spencer B J, Davis S H and Voorhees P W 1993 Morphological instability in epitaxially strained dislocation-free solid films: linear stability theory *J. Appl. Phys.* **73** 4955–70
[175] Spencer B J, Davis S H and Voorhees P W 1993 Morphological instability in epitaxially strained dislocation-free solid films: nonlinear evolution *Phys. Rev.* B **47** 9760–77
[176] Golovin A A, Davis S H and Voorhees P W 2003 Self-organization of quantum dots in epitaxially strained solid films *Phys. Rev.* E **68** 056203
[177] Ratsch C, Smilauer P, Vvedensky D D and Zangwill A 1996 Mechanism for coherent island formation during heteroepitaxy *J. Physique* I **6** 575–81
[178] Kurtz T G 1976 Limit theorems and diffusion approximations for density dependent Markov chains *Math. Program. Stud.* **5** 67–78
[179] Kurtz T G 1978 Strong approximation theorems for density dependent Markov chains *Stoch. Process. Appl.* **6** 223–40
[180] Fox R F and Keizer J 1991 Amplification of intrinsic fluctuations by chaotic dynamics in physical systems *Phys. Rev.* A **43** 1709–20
[181] Vvedensky D D, Zangwill A, Luse C N and Wilby M R 1993 Stochastic equations of motion for epitaxial growth *Phys. Rev.* E **48** 852–62
[182] Vvedensky D D 2003 Edwards–Wilkinson equation from lattice transition rules *Phys. Rev.* E **67** 025102
[183] Vvedensky D D 2003 Crossover and universality in the Wolf–Villain model *Phys. Rev.* E **68** 010601
[184] Villain J 1991 Continuum models of crystal growth from atomic beams with and without desorption *J. Physique* I **1** 19–42
[185] Lai Z W and Das Sarma S 1991 Kinetic growth with surface relaxation: continuum versus atomistic models *Phys. Rev. Lett.* **66** 2348–51
[186] Ballestad A, Ruck B J, Schmid J H, Adamcyk M, Nodwell E, Nicoll C and Tiedje T 2002 Surface morphology of GaAs during molecular beam epitaxy growth: comparison of experimental data with simulations based on continuum growth equations *Phys. Rev.* B **65** 205302
[187] Kan H-C, Shah S, Tadyyon-Eslami T and Phaneuf R J 2004 Transient evolution of surface roughness on patterned GaAs(001) during homoepitaxial growth *Phys. Rev. Lett.* **92** 146101
[188] Bimberg D, Grundmann M and Ledentsov N N 1999 *Quantum Dot Heterostructures* (New York: Wiley)
[189] Grundmann M (ed) 2002 *Nano-Optoelectronics: Concepts, Physics, and Devices* (New York: Springer)
[190] Loss D and DiVincenzo D P 1998 Quantum computation with quantum dots *Phys. Rev.* A **57** 120–6
[191] Shchukin V A and Bimberg D 1999 Spontaneous ordering of nanostructures on crystal surfaces *Rev. Mod. Phys.* **71** 1125–71
[192] Politi P, Grenet G, Marty A, Ponchet A and Villain J 2000 Instabilities in crystal growth by atomic or molecular beams *Phys. Rep.* **324** 271–404
[193] Hartmann A, Ducommun Y, Leifer K and Kapon E 1999 Structure and optical properties of semiconductor quantum nanostructures self-formed in inverted tetrahedral pyramids *J. Phys.: Condens. Matter* **11** 5901–15
[194] Alchalabi K, Zimin D, Kostorz G and Zogg H 2003 Self-assembled semiconductor quantum dots with nearly uniform sizes *Phys. Rev. Lett.* **90** 026104

[195] Tersoff J, Teichert C and Lagally M G 1996 Self-organization in growth of quantum dot superlattices *Phys. Rev. Lett.* **76** 1675–8
[196] Su X, Kalia R K, Nakano A, Vashishta P and Madhukar A 2003 InAs/GaAs square nanomesas: multimillion-atom molecular dynamics simulations on parallel computers *J. Appl. Phys.* **94** 6762–73
[197] Lam C and Sander L M 1993 Inverse method for interface problems *Phys. Rev. Lett.* **71** 561–4
[198] Frantziskonis G and Deymier P A 2000 Wavelet methods for analysing and bridging simulations at complementary scales: the compound wavelet matrix and application to microstructure evolution *Modelling Simul. Mater. Sci. Eng.* **8** 649–64
[199] Ismail A E, Rutledge G C and Stephanopoulos G 2003 Multiresolution analysis in statistical mechanics: I. Using wavelets to calculate thermodynamic properties *J. Chem. Phys.* **118** 4414–23
[200] Ismail A E, Stephanopoulos G and Rutledge G C 2003 Multiresolution analysis in statistical mechanics: II. The wavelet transform as a basis for Monte Carlo simulations on lattices *J. Chem. Phys.* **118** 4424–31
[201] Lee S-H, Moritz W and Scheffler M 2000 GaAs(001) surface under conditions of low As pressure: evidence for a novel surface geometry *Phys. Rev. Lett.* **85** 3890–3
[202] Schmidt W G, Mirbt S and Bechstedt F 2000 Surface phase diagram of (2×4) and (4×2) reconstructions of GaAs(001) *Phys. Rev.* B **62** 8087–91
[203] Ratsch C, Barvosa-Carter W, Grosse F, Owen J H G and Zinck J J 2000 Surface reconstructions for InAs(001) studied with density-functional theory and STM *Phys. Rev.* B **62** R7719–22
[204] Ratsch C 2001 Strain-induced change of surface reconstructions for InAs(001) *Phys. Rev.* B **63** 161306(R)
[205] Penev E, Kratzer P and Scheffler M 2001 Effect of strain on surface diffusion in semiconductor heteroepitaxy *Phys. Rev.* B **64** 085401
[206] Kratzer P, Penev E and Scheffler M 2003 Understanding the growth mechanisms of GaAs and InGaAs thin films by employing first-principles calculations *Appl. Surf. Sci.* **216** 436–46
[207] Leonard D, Pond K and Petroff P M 1994 Critical layer thickness for self-assembled InAs islands on GaAs *Phys. Rev.* B **50** 11687–92
[208] Kobayashi N P, Ramachandran T R, Chen P and Madhukar A 1996 *In situ* atomic force microscope studies of the evolution of InAs three-dimensional islands on GaAs(001) *Appl. Phys. Lett.* **68** 3299–301
[209] Dobbs H T, Vvedensky D D, Zangwill A, Johansson J, Carlsson N and Seifert W 1997 Mean-field theory of quantum dot formation *Phys. Rev. Lett.* **79** 897–900
[210] Dobbs H T, Zangwill A and Vvedensky D D 1998 Nucleation and growth of coherent quantum dots: a mean field theory *Surface Diffusion: Atomistic and Collective Processes* ed M Tringides (New York: Plenum) pp 263–75
[211] Madhukar A 1996 A unified atomistic and kinetic framework for growth front morphology evolution and defect initiation in strained epitaxy *J. Cryst. Growth* **163** 149–64
[212] Koduvely H M and Zangwill A 1999 Epitaxial growth kinetics with interacting coherent islands *Phys. Rev.* B **60** R2204–7
[213] Kratzer P, Penev E and Scheffler M 2002 First-principles studies of kinetics in epitaxial growth of III–V semiconductors *Appl. Phys.* A **75** 79–88
[214] Dodson B W and Taylor P A 1986 Monte Carlo simulation of continuous-space crystal growth *Phys. Rev.* B **34** 2112–5
[215] Faux D A, Gaynor G, Carson C L, Hall C K and Bernholc J 1990 Computer simulation studies of the growth of strained layers by molecular-beam epitaxy *Phys. Rev.* B **42** 2914–22
[216] LeGoues F K 1996 The effect of strain on the formation of dislocations at the SiGe/Si interface *Mater. Res. Soc. Bull.* **21** 38–44
[217] Joyce B A, Sudijono J L, Belk J G, Yamaguchi H, Zhang X M, Dobbs H T, Zangwill A, Vvedensky D D and Jones T S 1997 A scanning tunneling microscopy–reflection high-energy electron-diffraction–rate equation study of the molecular beam epitaxial growth of InAs on GaAs(001), (110) and (111)A—quantum dots and two-dimensional modes *Japan. J. Appl. Phys.* **36** 4111–7
[218] Much F, Ahr M, Biehl M and Kinzel W 2001 Kinetic Monte Carlo simulations of dislocations in heteroepitaxial growth *Europhys. Lett.* **56** 791–6
[219] Biehl M and Much F 2003 Simulation of wetting-layer and island formation in heteroepitaxial growth *Europhys. Lett.* **63** 14–20
[220] Haselwandter C and Vvedensky D D, unpublished